Atmos. Chem. Phys., 16, 15075–15095, 2016
www.atmos-chem-phys.net/16/15075/2016/
doi:10.5194/acp-16-15075-2016

Atmospheric Chemistry and Physics Open Access EGU

Heterogeneous ice nucleation on dust particles sourced from nine deserts worldwide – Part 1: Immersion freezing

Yvonne Boose[1,a], André Welti[1,b], James Atkinson[1], Fabiola Ramelli[1], Anja Danielczok[2], Heinz G. Bingemer[2], Michael Plötze[3], Berko Sierau[1], Zamin A. Kanji[1], and Ulrike Lohmann[1]

[1]Institute for Atmospheric and Climate Science, ETH Zurich, Zurich, Switzerland
[2]Institute for Atmospheric and Environmental Sciences, J. W. Goethe-University, Frankfurt am Main, Germany
[3]Institute for Geotechnical Engineering, ETH Zurich, Zurich, Switzerland
[a]now at: Institute for Meteorology and Climate Research, Karlsruhe Institute of Technology, Garmisch-Partenkirchen, Germany
[b]now at: Leibniz Institute for Tropospheric Research, Leipzig, Germany

Correspondence to: Yvonne Boose (yvonne.boose@env.ethz.ch) and Zamin A. Kanji (zamin.kanji@env.ethz.ch)

Received: 21 May 2016 – Published in Atmos. Chem. Phys. Discuss.: 2 June 2016
Revised: 26 September 2016 – Accepted: 14 October 2016 – Published: 6 December 2016

Abstract. Desert dust is one of the most abundant ice nucleating particle types in the atmosphere. Traditionally, clay minerals were assumed to determine the ice nucleation ability of desert dust and constituted the focus of ice nucleation studies over several decades. Recently some feldspar species were identified to be ice active at much higher temperatures than clay minerals, redirecting studies to investigate the contribution of feldspar to ice nucleation on desert dust. However, so far no study has shown the atmospheric relevance of this mineral phase.

For this study four dust samples were collected after airborne transport in the troposphere from the Sahara to different locations (Crete, the Peloponnese, Canary Islands, and the Sinai Peninsula). Additionally, 11 dust samples were collected from the surface from nine of the biggest deserts worldwide. The samples were used to study the ice nucleation behavior specific to different desert dusts. Furthermore, we investigated how representative surface-collected dust is for the atmosphere by comparing to the ice nucleation activity of the airborne samples. We used the IMCA-ZINC setup to form droplets on single aerosol particles which were subsequently exposed to temperatures between 233 and 250 K. Dust particles were collected in parallel on filters for offline cold-stage ice nucleation experiments at 253–263 K. To help the interpretation of the ice nucleation experiments the mineralogical composition of the dusts was investigated. We find that a higher ice nucleation activity in a given sample at 253 K can be attributed to the K-feldspar content present in this sample, whereas at temperatures between 238 and 245 K it is attributed to the sum of feldspar and quartz content present. A high clay content, in contrast, is associated with lower ice nucleation activity. This confirms the importance of feldspar above 250 K and the role of quartz and feldspars determining the ice nucleation activities at lower temperatures as found by earlier studies for monomineral dusts. The airborne samples show on average a lower ice nucleation activity than the surface-collected ones. Furthermore, we find that under certain conditions milling can lead to a decrease in the ice nucleation ability of polymineral samples due to the different hardness and cleavage of individual mineral phases causing an increase of minerals with low ice nucleation ability in the atmospherically relevant size fraction. Comparison of our data set to an existing desert dust parameterization confirms its applicability for climate models. Our results suggest that for an improved prediction of the ice nucleation ability of desert dust in the atmosphere, the modeling of emission and atmospheric transport of the feldspar and quartz mineral phases would be key, while other minerals are only of minor importance.

Published by Copernicus Publications on behalf of the European Geosciences Union.

1 Introduction

Predicting the occurrence and evolution of clouds at temperatures (T) below 273 K remains a challenge for global and regional climate models (Boucher et al., 2013). One source of uncertainty is the effect of certain aerosol particles which influence the cold cloud microphysics by acting as ice nucleating particles (INPs). Ice formation affects precipitation, cloud lifetime, and radiative properties of these clouds and, thus, global climate (Lohmann and Feichter, 2005). Mineral dust particles have been known as efficient INPs at $T \leq 253$ K for more than 60 years (e.g., Isono, 1955, and references given in Hoose and Möhler, 2012; Murray et al., 2012) and have been observed to nucleate ice in the atmosphere in various regions worldwide (Kumai, 1976; DeMott et al., 2003; Chou et al., 2011; Boose et al., 2016a, b). However, the molecular mechanisms and particle properties triggering ice nucleation on atmospheric mineral dusts are still the subject of ongoing research. Supercooled cloud droplets can freeze homogeneously at temperatures below 235 K, without the aid of an INP (Schaefer, 1946; Mason and Ludlam, 1950). At higher temperatures the surface of an INP is required to overcome the energy barrier of freezing. Traditionally, four pathways of ice nucleation are differentiated (Vali et al., 2015):

1. deposition nucleation, where ice forms on an INP directly from the vapor phase;
2. condensation freezing, in which ice forms during the process of water condensing on an INP;
3. immersion freezing, where an INP immersed in a supercooled cloud droplet initiates freezing;
4. contact freezing, where the interaction of an INP with the surface of a supercooled droplet either from the outside or inside of the droplet leads to freezing.

Ice formation in clouds with top temperatures above 263 K is often observed (Hobbs and Rangno, 1985), but only very few aerosol particle types have been identified to nucleate ice at these warm temperatures. These are mainly biological particles, such as certain bacterial strains or macromolecules (Schnell and Vali, 1976; Krog et al., 1979; Möhler et al., 2008b; Pummer et al., 2012). The ice nucleation ability of soot (Brooks et al., 2014; Kulkarni et al., 2016) at heterogeneous freezing temperatures is still debated as contradicting results were observed, spanning from hardly any ice nucleation ability at $T > 236$ K (Kanji et al., 2011) to up to 3 % of soot particles active in the immersion mode (DeMott, 1990). Similarly, the reported freezing behavior of secondary organic aerosol particles varies from inefficient to comparably efficient (Möhler et al., 2008a; Prenni et al., 2009; Wang et al., 2012; Ladino et al., 2014; Ignatius et al., 2016). Aerosol particles from marine sources are believed to be important INP at remote locations and are subject of current research (Knopf et al., 2011, 2014; DeMott et al., 2015a; Wilson et al., 2015). Recently, the K-feldspar microcline and the Na-feldspar albite, both minerals found in atmospheric dust, have been identified to nucleate ice at temperatures up to 271 K (Harrison et al., 2016).

For the implementation of ice nucleation into climate models, a simplistic description of ice formation on different INP types is required. Existing parameterizations for dust can be based on laboratory experiments using commercially available dusts such as Arizona Test Dust (ATD) including mostly pure clay mineral samples such as illite, kaolinite, and montmorillonite (Lüönd et al., 2010; Murray et al., 2011; Niedermeier et al., 2011), dust samples collected from the surface (Niemand et al., 2012), or on in situ measurements in the atmosphere at locations often distant from major dust sources (DeMott et al., 2010; Tobo et al., 2013). One recent study by DeMott et al. (2015b) combines laboratory data of two surface-collected dust samples with results from two flight campaigns over the Pacific Ocean and the Caribbean Sea within dust layers that underwent long-range transport from Asia and the Sahara, respectively. The authors found relatively good agreement amongst the different samples. They concluded that both a parameterization from Niemand et al. (2012) as well as one adapted from Tobo et al. (2013) were applicable for predicting atmospheric mineral dust INP concentrations.

For laboratory ice nucleation experiments, dust samples collected from the surface typically have to be sieved or milled, which may break up larger agglomerates and alter the size-dependent mineralogy (Perlwitz et al., 2015). This could significantly alter the ice nucleation ability of these dust particles in laboratory experiments compared to their ambient ice nucleation ability. It has been shown that milling of hematite or quartz particles leads to an increase in ice nucleation efficiency compared to the unmilled samples (Hiranuma et al., 2014; Zolles et al., 2015). It has been speculated that this is also part of the reason for ATD, a commercially available dust sample that is washed and milled after collection from a certain desert area in Arizona, being more ice nucleation active than natural unprocessed dust samples (Möhler et al., 2006).

Due to their high abundance, for many decades the immersion freezing behavior of atmospheric dust was attributed largely to clay minerals and ice nucleation on relatively pure clay mineral samples was often studied in more detail (Hoffer, 1961; Lüönd et al., 2010; Murray et al., 2010, 2011; Broadley et al., 2012; Pinti et al., 2012; Welti et al., 2012; Hiranuma et al., 2015). Recently, Atkinson et al. (2013) showed that compared to other minerals, feldspar particles are more efficient immersion mode INPs at temperatures above 245 K. The K-feldspars (microcline, orthoclase, and sanidine) were found to be more ice nucleation active than the Na / Ca-feldspars albite, anorthite, and other plagioclase feldspars (Atkinson et al., 2013; Zolles et al., 2015; Peckhaus et al., 2016). Amongst the K-feldspars microcline appears to be the

most ice nucleation active (Augustin-Bauditz et al., 2014; Kaufmann et al., 2016), even nucleating ice at a temperature of 271 K (Harrison et al., 2016). Feldspar is a highly complex group of minerals and, depending on the source, mineralogically similar samples can have different ice nucleation abilities (Harrison et al., 2016). Thus it remains an open question if and how feldspar is affecting the ice nucleation behavior of dust in the atmosphere and if it is causing ice nucleation in clouds at $T > 263$ K. A high variability in ice nucleation activity was found for quartz, with some quartz samples being more ice nucleation active in the immersion mode than clay minerals but always less than the feldspars (Atkinson et al., 2013; Zolles et al., 2015; Kaufmann et al., 2016). It is suspected that functional groups on the surface of feldspars and quartz are responsible for their higher ice nucleation ability (Zolles et al., 2015) but it is unknown where the high variability stems from. Quartz is commonly (5–50 wt %) found in atmospherically transported Saharan dust samples (Avila et al., 1997; Caquineau et al., 1998; Alastuey et al., 2005; Kandler et al., 2009). A recent study by Kaufmann et al. (2016) investigated the ice nucleation ability of surface-collected samples from eight different arid regions worldwide and several single-mineral reference samples using differential scanning calorimetry. The authors found at maximum a 6 K spread in freezing temperatures of emulsion experiments amongst surface-collected samples from different atmospheric dust source regions. They confirmed the exceptional freezing ability of microcline but found only a minor fraction (4 wt %) in one of the samples from the dust source regions studied. Their samples contained quartz fractions between 1 and 26 wt %, K-feldspar fractions between 0 and 10 wt %, and plagioclase fractions between 0 and 22 wt %.

It has been observed that the size distribution of dust changes during its emission and transport compared to dust on the surface. This leads to variations in the mineralogical composition of the dust (D'Almeida and Schütz, 1983; Murray et al., 2012; Knippertz and Stuut, 2014), as the mineralogical composition is size dependent due to differences in the hardness, cleavage, shape, and reactivity of minerals. Hard minerals such as feldspar tend to be dominant in the large grains whereas soft minerals are concentrated in the small size fraction (e.g., clay minerals). Saltation and dust emission strength depend on several factors and are nonlinear in dust particle size (Knippertz and Stuut, 2014). During atmospheric transport, gravitational settling or wet deposition further alters the size distribution. Additionally, minerals which act as cloud condensation nuclei or INPs are preferably lost.

Airborne dust particles smaller than 20 µm over the North Pacific have been found to contain 10 to over 50 wt % clay minerals such as illite, kaolinite, or smectite, 4–40 wt % quartz, and 4–75 wt % plagioclase feldspar (Leinen et al., 1994). Kandler et al. (2009) found that dust particles over Morocco consist of about 30 wt % clay minerals (illite, kaolinite, chlorite), less than 5 wt % plagioclase but over 20 wt % K-feldspar, less than 10 wt % quartz, and less than 10 wt % calcite in the size range below about 20 µm geometric diameter. Other identified minerals in the airborne dust were rutile, gypsum, dolomite, hematite, or halite. Similar results were found by Falkovich et al. (2001) over Israel. Caquineau et al. (1998) found a north–south gradient of the illite to kaolinite ratio of soil samples in the Sahara with higher values in the northern and western part of the Sahara and lower values in the southern and central Sahara.

Non-mineral matter, which can become internally or externally mixed with the mineral dust before or after emission, may affect the ice nucleating behavior of the dust. Sulfuric acid (Sullivan et al., 2010; Augustin-Bauditz et al., 2014) or secondary organic aerosol coating (Möhler et al., 2008a) has been observed to decrease the ice nucleating ability while exposure to ozone (Kanji et al., 2013) or the presence of ammonium sulfate (Boose et al., 2016b) has been suggested to improve it. Biological material can adsorb to mineral dust, enhancing its ice nucleating ability (Schnell, 1977; Conen et al., 2011; O'Sullivan et al., 2016).

In this study we investigate the immersion ice nucleation properties of 15 dust samples from nine different deserts around the world. Four of the samples were collected directly from the air (Tenerife) or by deposition after atmospheric transport (Crete, Egypt, Peloponnese) for subsequent analysis in the laboratory without additional treatment such as sieving or milling. Based on back trajectory analysis, the four airborne samples originate from different parts of the Sahara. The ice nucleation ability of these airborne dusts was compared to that of several samples collected in the desert. The effect of sieving and milling on the ice nucleation behavior of two surface-collected samples was investigated.

Immersion mode ice nucleation measurements at temperatures between 235 and 250 K were conducted with the combination of the Zurich Ice Nucleation Chamber, ZINC (Stetzer et al., 2008), and the Immersion Mode Cooling chAmber, IMCA (Lüönd et al., 2010). Particles of four dust samples were collected on filters for subsequent offline analysis with the Frankfurt Ice Deposition Freezing Experiment (FRIDGE) counter operated in the droplet freezing mode as described by Ardon-Dryer and Levin (2014) and Hiranuma et al. (2015). This allowed examination of immersion freezing at temperatures between 250 and 262 K, covering a wider range of heterogeneous freezing temperatures than would otherwise be possible with IMCA-ZINC alone. The aim of the current study, as well as a follow-up study on deposition/condensation nucleation, is to investigate the link between ice nucleation and bulk mineralogy of desert dust as it is found in the atmosphere and to compare it to surface-collected samples. By using aeolian transported samples, the particle size distribution and sample composition are as realistic as possible. To our knowledge this is the first study to investigate ice nucleation behavior of airborne desert dust in the laboratory, compare it with surface-collected natural dust samples, and link it to the mineralogical composition

of these complex samples. With samples from nine different deserts we present a data set covering most major global dust sources.

2 Methods

2.1 Dust sample origins and processing

The immersion mode freezing behavior of a total of 15 different dust samples was investigated. The collection sites are shown in Fig. 1 together with the major dust emission sources and common atmospheric transport pathways. GPS coordinates of the collection sites are provided in the Supplement. It can be seen from Fig. 1 that the dust samples stem from most of the major atmospheric dust sources. The Tenerife sample was collected directly from the air over 4 days in August 2013 at the Izaña observatory on Tenerife, Spain, using a custom-made large cyclone (Advanced Cyclone Systems, S.A.: flow rate of 200 $m^3 h^{-1}$ and D_{50} = 1.3 µm, the diameter at which the collection efficiency is 50 %). After deposition on a roof and on solar panels, dust samples were collected at the Aburdees observatory, Egypt, on 10 May 2010 and in Crete and the Peloponnese in Greece in April 2014. The Crete sample was an integrated sample over several dust events whereas the Peloponnese sample was from one single dust event. Surface collection sites were (i) the Atacama desert in Chile; (ii) a location approximately 70 km from Uluru in Australia; (iii) the Great Basin in Nevada and (iv) the Mojave desert in California, USA; (v) a Wadi in the Negev desert, approximately 5 km from Sde Boker in Israel; (vi) dunes in the Sahara, close to Merzouga in Morocco; (vii) dunes in the Arabian desert in Dubai; (viii) the Etosha pan in Namibia, a dry salt pan; and (ix) the Taklamakan desert in China. The Israel sample and the Etosha sample are from the same batch as those studied in Kaufmann et al. (2016).

The surface-collected samples needed to be sieved to separate the grain sizes larger than 32 µm from the remaining sample to avoid clogging of the aerosol generation system used for the ice nucleation experiments. Samples were sieved in a cascade of dry sieves with the smallest cutoff size being at 32 µm diameter (Retsch Vibratory Sieve Shaker AS 200). Typically only a few weight percent of the sample was in this size range. The Australia and Morocco samples had no fraction in this size range and thus were milled using a vibratory disc mill (Retsch, model RS1). For the Morocco sample, particles of the lowest size bin (32 to 64 µm) were milled. The Australia sample was first sieved with a coarse, millimeter-range sieve to separate any large material, and the remaining sand was milled. For the Atacama and Israel samples, both a milled and a sieved sample were compared to investigate the effect of milling on ice nucleation. In case of the Atacama sample, part of the unsieved sample was milled. The Israel sample was first sieved and part of the sieved sample with $d \leq 32$ µm was milled. The sub-32 µm size fraction of the other samples was too small to investigate the milling effect. The composition of natural dust samples is presumed to be heterogeneous, i.e., external and internal mixtures of different minerals and potentially containing organic or biological material (Meola et al., 2015). Additionally, they have probably undergone natural aging processes due to the exposure to the atmosphere of the surface-collected samples and actual atmospheric aging of the airborne samples (Dall'Osto et al., 2010). This could physically or chemically alter the surface of the dust particles, potentially changing the ice nucleation properties compared to the pure mineral dust particles. Effects of washing or heating of the samples, which could yield information on coating or mixing, could not be investigated in this part of the study due to the small sample size of the airborne samples.

2.2 Dust particle generation

The dust samples were dry dispersed into a 2.78 m^3 stainless steel aerosol reservoir tank (Kanji et al., 2013) using a Rotating Brush Generator (RBG, Palas, model RBG 1000) with N_2 (5.0) as carrier gas via a cyclone that confined the dust size distribution to below $D_{50} = 2.5$ µm. The maximum particle concentration in the tank was about 1200 cm^{-3} and decreased steadily to about 300 cm^{-3} over approximately 10 h. Before each experiment, the tank was cleaned by repeatedly evacuating and purging it with N_2 until the particle concentration decreased to 30–90 cm^{-3}. The total particle concentration was monitored with a condensation particle counter (CPC; TSI model 3772). The ice nucleating particle counters, the particle collection for offline FRIDGE experiments and the instruments measuring the particles' size distribution sampled directly from the tank. For the IMCA-ZINC measurements, the particle concentration was diluted to about 60 cm^{-3} to avoid coincidence effects in the detector which occur if more than one particle is present in the laser beam of the detector (Nicolet et al., 2010).

2.3 Aerosol particle size distribution

The particle size distribution in the reservoir tank was monitored using a scanning mobility particle sizer (SMPS; TSI, DMA model 3081, CPC model 3010) for mobility diameters (d_m) between 12.2 and 615 nm and an Aerodynamic Particle Sizer (APS; TSI, model 3321) for aerodynamic diameters (d_{aer}) between 0.5 and 20 µm. After converting the mobility and aerodynamic diameter to volume equivalent diameter (d_{ve}), the size distributions were merged. A shape factor of $\chi = 1.36$ and a particle density of $\rho = 2.65$ g cm^{-3} were assumed for the conversion. These values lie in the range of natural dust samples analyzed in earlier studies; e.g., for quartz, $\chi = 1.10$–1.36 (Hinds, 1999; Alexander, 2015) and $\rho = 2.6$ g cm^{-3} (Hinds, 1999; Kandler et al., 2007), and for illite NX, $\chi = 1.49$ and $\rho = 2.65$ g cm^{-3} (Hiranuma et al.,

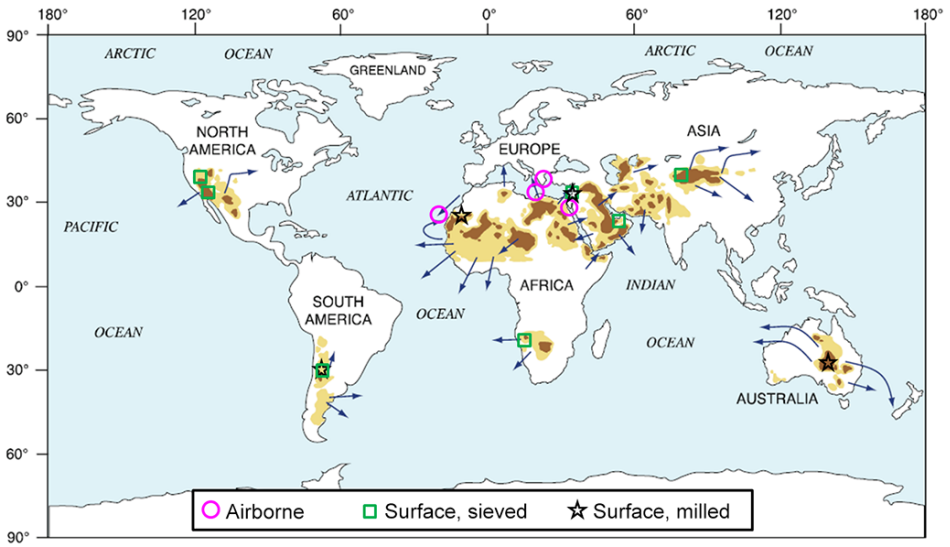

Figure 1. Collection sites of the dust samples. Green squares/black stars indicate sieved/milled samples which were collected directly from the surface; pink circles indicate samples that were collected either directly from the air or by deposition after transport from the Sahara. See text for details on the collection methods and treatment after collection. The map was adapted from Knippertz and Stuut (2014) and is based on data from Total Ozone Mapping Spectrometer (TOMS) satellite data of the absorbing aerosol index (AAI). Dark brown color indicates 21–31 days of AAI > 0.7, corresponding to significant amounts of dust or smoke. Yellow indicates 7–21 days of AAI > 0.7. Arrows show typical dust transport pathways in the atmosphere.

2015). Assuming spherical particles, the area size distribution was calculated and fitted with a bimodal lognormal distribution. The mean particle surface area ($\overline{A_{ve,w}}$) was calculated from the resulting fit for each sample (see Table 1) as well as the corresponding surface area-weighted mean diameter ($\overline{d_{ve,w}}$). Over the course of a single experiment the size distribution changed as larger particles settle out of the volume faster than smaller ones. This effect was reduced by a fan inside the aerosol tank leading to $\overline{A_{ve,w}}$ varying by 6 to 24 % over the course of an experiment for the different samples, except for the Great Basin sample (64 %), which was coarser than the other samples and settled out faster.

Figure 2 shows a schematic of the different size fractions resulting from the different collection methods and post-treatment (sieving/milling) of the samples used for ice nucleation experiments in the tank and the mineralogical analysis. Due to the small amount of sample, a mineralogical analysis of the identical size fraction as in the tank (< 2.5 µm) was not possible. Instead, we used the entire size fraction of the airborne samples, the smallest size fraction of the sieved samples (< 32 µm), and the whole size distribution of the milled samples after milling.

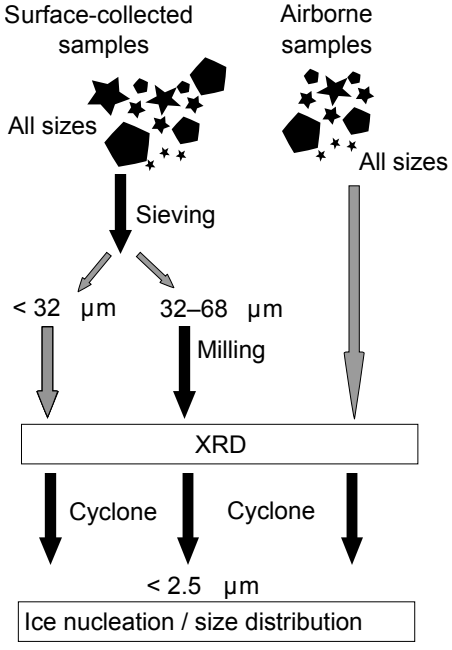

Figure 2. Schematic of size fractions used for XRD and ice nucleation.

2.4 Mineralogy analysis

The quantitative mineralogical composition of the bulk dust samples was investigated using the X-ray diffraction (XRD) Rietveld method (Rietveld, 1969) using a Bragg–Brentano diffractometer (Bruker AXS D8 Advance with CoKalpha radiation). The qualitative phase composition was determined with the software DIFFRACplus (Bruker AXS). On the basis of the peak positions and their relative intensities, the mineral phases were identified in comparison to the PDF-2 data base (International Centre for Diffraction Data). The quanti-

Table 1. Overview of the dust size distribution parameters: the mean particle surface area per particle $\overline{A_{ve,w}}$ with relative error $\delta(\overline{A_{ve,w}})$ and the corresponding diameter of a particle with this surface area ($\overline{d_{ve,w}}$) with the relative error $\delta(\overline{d_{ve,w}})$.

Sample number	Collection site	Type	$\overline{A_{ve,w}}$ (µm^2)	$\delta(\overline{A_{ve,w}})$	$\overline{d_{ve,w}}$ (nm)	$\delta(\overline{d_{ve,w}})$
1	Atacama	sieved	2.79	0.17	940	0.08
2	Atacama	milled	2.56	0.24	897	0.11
3	Australia	milled	2.14	0.09	824	0.05
4	Crete	airborne	3.04	0.08	983	0.04
5	Dubai	sieved	2.18	0.18	830	0.09
6	Egypt	airborne	3.26	0.12	1017	0.06
7	Etosha	sieved	2.08	0.07	813	0.03
8	Great Basin	sieved	16.4	0.64	2133	0.39
9	Israel	sieved	3.32	0.14	1024	0.07
10	Israel	milled	2.57	0.12	904	0.06
11	Mojave	sieved	2.99	0.14	973	0.07
12	Morocco	milled	2.81	0.13	960	0.07
13	Peloponnese	airborne	3.27	0.06	1020	0.03
14	Taklamakan	sieved	3.69	0.19	1079	0.09
15	Tenerife	airborne	3.55	0.12	1061	0.06

tative composition was calculated by means of Rietveld analysis of the XRD pattern (Rietveld program AutoQuan, GE SEIFERT; Bergmann et al., 1998; Bish and Plötze, 2011).

The results and uncertainties for the mineralogy of each sample given from the Rietveld refinement are provided in Tables 2 and 3. For the Egypt sample the mineralogical composition is associated with a significantly higher uncertainty because the amount of sample was small and the measured intensity of the diffracted X-rays very low. In this case the grain statistics were poor and crystals more likely to be arranged in a certain, preferred orientation instead of randomly, leading to a potential overestimation of some mineral fractions. Similarly, the milling of the Israel sample likely interfered with the preferred orientation of the minor components in the sieved samples, leading to an observed reduction of these mineral fractions (e.g., illite, dolomite, plagioclase) in the milled compared to the sieved sample. The differentiation between the microcline and orthoclase K-feldspar fraction was for some samples not possible (i.e., Morocco and Australia) where both phases were likely present. In case of a low K-feldspar content of a few wt % it was not possible to determine if K-feldspar was present as microcline, orthoclase or sanidine or a mixture of the different phases. Values are given for the K-feldspar with the best Rietveld fit result. As Rietveld fit results for the various Na-plagioclase feldspars (albite, oligoclase and andesine) were often insignificantly different, they are summarized as Na-plagioclase. The fractions of ankerite and dolomite are usually provided together because in some cases (especially Morocco) it was not possible to differentiate between them. Only for the Etosha sample are they provided separately because the fractions were large enough to be distinguishable (Kaufmann et al., 2016).

Due to the broader size range of particles studied with XRD, the mineralogy describes not only the particles that were studied with the ice nucleation chambers but also the fraction between 2.5 and 32 µm. This could lead to differences between the measured mineralogy and the actual mineralogical composition of particles smaller than 2.5 µm due to differences in the hardness and cleavage or fracture, i.e., the breaking behavior, of different minerals. This is particularly true for softer minerals such as calcite, which has a Mohs hardness of 3 (standard scale of hardness between 1, talc, and 10, diamond), and clay minerals (2–2.5) in contrast to feldspars (6) and quartz (7), as well as for minerals with a higher cleavage such as gypsum and calcite (perfect cleavage) compared to quartz (without cleavage; for information on mineral cleavage and hardness see www.mindat.org or www.webmineral.com). Natural mechanical weathering thus likely has enhanced the clay mineral and calcite content in the smaller particle fraction whereas feldspars and quartz tend to be found in the larger size fractions. For each filling of the reservoir tank a similar volume of dust sample was used ($\approx 0.2\,\mathrm{cm}^3$) and the dust density is assumed to be comparable (about $2.65\,\mathrm{g\,cm}^{-3}$). This allows us to roughly approximate what fraction of particles was larger than 2.5 µm by the amount of dust sample left over in the 2.5 µm cutoff cyclone and the particle concentration reached in the tank. Hardly any particles were left over in the cyclone and maximum particle concentrations of 900–1200 cm^{-3} were reached by all milled samples apart from the Morocco sample and by all airborne samples apart from the Egypt sample. We suspect that the Egypt sample has a higher fraction of large particles because it originated from local sources within Egypt and thus the transport time was much shorter compared to the other airborne samples leading to the size distribution

Table 2. Mineralogical composition in wt % and uncertainty from the Rietveld refinement (see text for details). Where microcline and orthoclase are present in the same sample, their individual fraction could not be distinguished reliably. Nevertheless, the best Rietveld fit results are given for orthoclase and microcline individually in these cases. The Etosha sample was taken from Kaufmann et al. (2016), who do not provide a Rietveld fit uncertainty from AutoQuan but estimate a 15 % accuracy.

Mineral type	Atacama sieved	Atacama milled	Australia milled	Crete airborne	Dubai sieved	Egypt airborne	Etosha sieved	Great Basin sieved
Ankerite							23	
Biotite		2.8 ± 0.6			1.0 ± 0.5			
Calcite				25.0 ± 0.6	37.2 ± 0.6	29.2 ± 1.2	29	12.9 ± 0.4
Chlorite				3.8 ± 0.6	14.0 ± 1.2	8.2 ± 1.3		2.1 ± 0.3
Cristobalite	12.7 ± 1.9	14.0 ± 1.7						
Dolomite				3.1 ± 0.7	6.8 ± 0.5	8.1 ± 1.3	27	1.9 ± 0.3
Gypsum				3.7 ± 0.7		5.5 ± 0.9		2.8 ± 0.3
Halite				1.0 ± 0.2		4.4 ± 0.5		2.1 ± 0.1
Hematite	4.0 ± 0.5	3.2 ± 0.4	0.6 ± 0.1	0.9 ± 0.2	1.4 ± 0.2			0.9 ± 0.2
Hornblende	1.3 ± 0.7	1.8 ± 0.6		1.5 ± 0.4	1.8 ± 0.5			1.0 ± 0.5
Illite	10.0 ± 1.0							
Kaolinite				12.4 ± 1.0		10.5 ± 1.5		17.7 ± 0.9
Microcline			3.9 ± 0.5					30.1 ± 0.8
Muscovite	4.2 ± 1.0	2.4 ± 0.6		9.0 ± 0.6	4.1 ± 0.5	7.6 ± 1.3	10	4.0 ± 0.5
Orthoclase	11.8 ± 0.9	22.3 ± 0.9	4.2 ± 0.5	5.1 ± 0.6	2.4 ± 0.4	3.5 ± 1.1		
Palygorskite				4.5 ± 0.5	3.4 ± 0.5			
Na-plagioclase	39.3 ± 1.6	43.2 ± 1.4		7.2 ± 0.4	9.5 ± 0.4			3.7 ± 0.3
Smectite							1	
Quartz	16.7 ± 0.6	10.4 ± 0.4	91.3 ± 0.5	23.0 ± 0.5	13.3 ± 0.3	23.0 ± 1.1	1	20.1 ± 0.5
others					5.1 ± 0.4		9	0.7 ± 0.3

Table 3. Mineralogical composition in wt % and uncertainty from the Rietveld refinement using AutoQuan continued. Where microcline and orthoclase are present in the same sample, their individual fraction could not be distinguished.

Mineral type	Israel sieved	Israel milled	Mojave sieved	Morocco milled	Peloponnese airborne	Taklamakan sieved	Tenerife airborne
Biotite							
Calcite	67.2 ± 1.2	81.0 ± 1.0	11.0 ± 0.5	6.0 ± 0.3	33.0 ± 0.6	14.6 ± 0.4	6.6 ± 0.3
Chlorite			7.5 ± 1.4	5.9 ± 1.0	2.7 ± 9.5	7.1 ± 0.9	1.6 ± 0.6
Cristobalite							
Dolomite/ankerite	8.0 ± 0.4	1.3 ± 0.2	9.0 ± 0.5	1.4 ± 0.6	4.6 ± 0.5	4.6 ± 0.5	2.2 ± 0.3
Gypsum	1.2 ± 0.2					1.8 ± 0.5	2.4 ± 0.3
Halite						0.9 ± 0.2	0.4 ± 0.1
Hematite	0.5 ± 0.1		0.7 ± 0.2	2.7 ± 0.5	0.6 ± 0.2		0.6 ± 0.1
Hornblende			0.6 ± 0.3		1.5 ± 0.5	5.4 ± 0.5	
Illite	4.2 ± 1.6	0.3 ± 0.2	8.0 ± 1.7	3.0 ± 0.7	12.5 ± 1.0		6.2 ± 0.8
Kaolinite	0.8 ± 0.6	0.3 ± 0.3			7.8 ± 0.7		15.6 ± 1.0
Microcline	1.7 ± 0.4	1.3 ± 0.4		3.8 ± 1.0			3.9 ± 0.5
Muscovite		1.1 ± 0.5	9.6 ± 0.7	1.8 ± 0.3	4.8 ± 0.8	8.0 ± 0.6	7.4 ± 0.6
Orthoclase			4.8 ± 0.4	2.2 ± 0.6	4.0 ± 0.5	5.3 ± 0.6	
Palygorskite	2.2 ± 0.4	1.6 ± 0.4			5.3 ± 0.8		4.1 ± 0.4
Na-plagioclase	2.3 ± 0.5	0.7 ± 0.3	10.0 ± 0.8	8.8 ± 0.4	5.0 ± 0.4	19.3 ± 0.8	3.5 ± 0.4
Smectite	4.5 ± 0.6	6.4 ± 1.2	26.1 ± 2.6				31.8 ± 1.5
Quartz	7.3 ± 0.3	6.1 ± 0.2	12.8 ± 0.5	63.8 ± 1.2	17.9 ± 0.4	33.1 ± 0.7	14 ± 0.4
Others			0.2 ± 0.1		0.5 ± 0.1		

being shifted to larger particles. Of the sieved samples, the Dubai, Great Basin, Israel, Mojave, and Taklamakan samples had a comparably high fraction of particles larger than 2.5 µm and particle concentrations of 400–970 cm^{-3} were reached when filling the tank. For these samples the presented mineralogy may not be fully representative for the

particles < 2.5 µm investigated for ice nucleation. In contrast, particles of the Etosha and Atacama sieved samples were mainly smaller than 2.5 µm and thus the mineralogy is representative of the small particle fraction. In summary, the identified mineralogical composition is well representative for the particle size fraction used for ice nucleation experiments on the Atacama milled and sieved, sieved Etosha, Israel milled, milled Australia, and the airborne Crete, Peloponnese, and Tenerife samples.

2.5 Immersion freezing experiments and data treatment

Immersion freezing experiments between 235 and 250 K were conducted by extending ZINC (Stetzer et al., 2008) with IMCA (Lüönd et al., 2010). ZINC is a vertically oriented continuous flow diffusion chamber (Rogers, 1988) with two flat parallel walls. The walls are ice coated before an experiment and by applying a temperature gradient between the two walls at supercooled temperatures supersaturation with respect to ice is established between the walls. To ensure droplet activation of all sampled particles before freezing, IMCA is installed upstream of ZINC. In IMCA a relative humidity of 120 % with respect to water at a temperature of 303 K is provided by humidified filter paper on the two parallel walls of the chamber. Under these conditions, all particles activate such that each droplet contains a single dust particle. The droplets are then cooled to the experimental temperature before they enter ZINC. For the immersion freezing experiments the relative humidity in ZINC is kept at water saturation. The IODE detector (Nicolet et al., 2010) measures the depolarization signal of a linearly polarized laser beam by the particles. This allows differentiation between spherical droplets, which nominally do not lead to a depolarization signal, and the non-spherical ice crystals which depolarize the laser light. The ratio of the detected ice crystal concentration (N_i) to the sum of ice crystals and detected droplet concentration (N_d) is called the frozen fraction (FF):

$$\mathrm{FF} = \frac{N_\mathrm{i}}{N_\mathrm{d} + N_\mathrm{i}}. \quad (1)$$

IODE can distinguish the depolarization signal of droplets and ice crystals between the limits of detection (LOD) of FF = 0.1 and FF = 0.9. Over the course of about 3 h the temperature is stepwise ramped up. Each data point represents 2000–3000 single detected particles.

For independent offline immersion freezing measurements between 250 and 263 K with FRIDGE, dust particles were collected by filtration from the tank over 3.5 h using Teflon membrane filters (Fluoropore PTFE, 47 mm, 0.2 µm, Merck Millipore Ltd.). The particles were then extracted from the filters into vials with 10 mL of deionized water for 10 minutes in an ultrasonic bath, and

150 drops of 0.5 µL each were randomly placed on a silicon plate on the cold stage of FRIDGE using an Eppendorf pipette. At ambient pressure conditions the temperature of the cold stage was then lowered by 1 K min^{-1} and the number of drops freezing as a function of temperature is recorded with a CCD camera. This process is repeated several times with fresh droplets until a minimum of 1000 droplets is exposed. The INP concentration is given by (Vali, 1971; Ardon-Dryer and Levin, 2014)

$$K'(T) = \frac{1}{V_\mathrm{drop}}[\ln(N_0) - \ln(N(T))]\frac{V_\mathrm{water}}{V_\mathrm{air}}, \quad (2)$$

where $K'(T)$ is the cumulative INP concentration, V_drop is the volume of a droplet, N_0 the number of droplets sampled, $N(T)$ the number of frozen droplets, V_water the volume of water used to wash off the particles from the filter, and V_air the volume of air (N_2 in the current study) sampled through the filter. The temperature uncertainty is ±0.2 K and the uncertainty in FF typically ±30 % at $T \leq 260$ K and decreases with lower temperatures.

Due to the small sample amounts particularly of the airborne dust samples, generating monodisperse particles for the ice nucleation measurements was not possible. Earlier studies have shown that the probability of a particle to act as INP scales with the surface area of the particle immersed in a droplet (Archuleta et al., 2005; Welti et al., 2009; Kanji and Abbatt, 2010). So-called ice-active sites (Vali, 1966) are assumed on the surface of an INP in the deterministic concept (Langham and Mason, 1958). The probability of such a site to be present on a particle increases with the surface area. To compare the FF measured in IMCA from samples with different size distributions, the FF is normalized by the mean aerosol particle surface area. This yields the ice-active surface site density, n_s:

$$n_\mathrm{s} = -\frac{\ln(1 - \mathrm{FF})}{\overline{A_\mathrm{ve,w}}}. \quad (3)$$

In the case of FRIDGE it is calculated as

$$n_\mathrm{s} = -\frac{\ln(1 - \frac{N(T)}{N_0})}{A_\mathrm{t,drop}}, \quad (4)$$

with $A_\mathrm{t,drop}$ being the total aerosol surface area present in each droplet and given as

$$A_\mathrm{t,drop} = \overline{N} V_\mathrm{air} \overline{A_\mathrm{ve,w}} \frac{V_\mathrm{water}}{V_\mathrm{drop}}, \quad (5)$$

with the mean total aerosol concentration $\overline{N}$ in the reservoir tank during the time of the particle collection as measured by the CPC. The assumption that active sites are uniformly distributed over individual particle surfaces, and therefore that n_s stays constant with particle size, most likely has limitations for complex polymineral samples such as desert dust

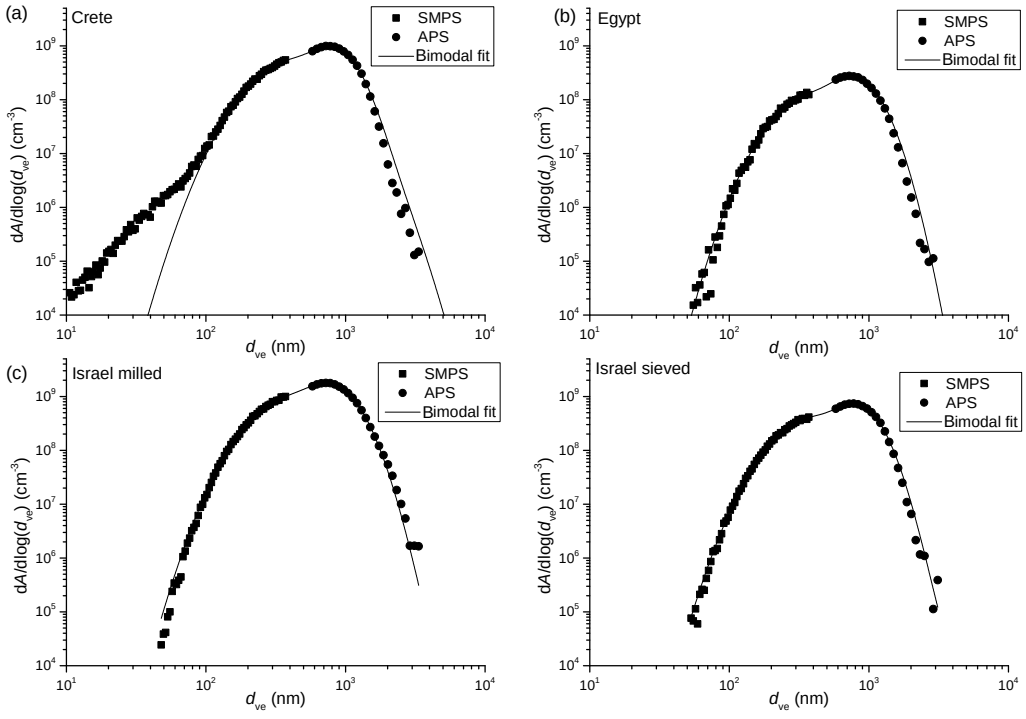

Figure 3. Sample surface area distribution of four of the dust samples with bimodal fits.

particles. Therefore, the provided n_s values should not be treated as an exact parameter, valid at any particle size, but rather a normalization method for the bulk natural dust samples $< 2.5\,\mu m$ which we investigated.

3 Results and discussion

3.1 Dust size distribution

Most of the size distributions of the different dust samples in the tank were bimodal. Figure 3 shows exemplary SMPS and APS surface area distribution data of four samples together with the bimodal fit. Since one mode was detected in each instrument's size range, the shape factor χ was optimized to give the best overlap of the two size distributions. For any shape factor within realistic limits for atmospheric dusts ($1.1 \leq \chi \leq 1.6$, Alexander, 2015) the two modes remained distinguishable. They are likely related to the high inhomogeneity of the samples with respect to hardness and fracture. Two airborne (Crete and Egypt), one surface-collected sieved, and one surface-collected milled (both Israel) samples are shown. The Crete sample has a third small mode at $d_{ve} = 50\,nm$. Since the smaller aerosol particles contribute only little to the average surface area, the distribution was also bi-modally fitted. The mean particle surface area values are given in Table 1 together with the relative error $\delta(\overline{A_{ve,w}})$ resulting from a change in distribution during the course of the experiment. All samples peak in number concentration between $d_{ve} = 200$ and 400 nm and a mean particle surface area of $\overline{A_{ve,w}} = 2$–$3.7\,\mu m^2$ corresponding to a diameter of $\overline{d_{ve,w}} = 800$–$1100\,nm$. Only the Great Basin sample differs strongly because of the presence of predominantly large particles leading to a high mean particle surface area ($\overline{A_{ve,w}} = 16.4\,\mu m^2$, $\overline{d_{ve,w}} = 2133\,nm$). The relative error $\delta(\overline{A_{ve,w}})$ is 64 % in the case of the Great Basin sample because two refills were necessary during the course of the experiment. For all other samples $\delta(\overline{A_{ve,w}})$ is less than 24 %.

3.2 Ice nucleation of desert dust

The plots on the left side of Fig. 4 show the FF as a function of temperature between 235 and 253 K, separately for non-Saharan and the Saharan samples. The majority of the non-Saharan FF curves (Fig. 4a and b) behave similarly, with two samples being distinctly different: the Australia sample shows significantly higher FF values at all temperatures, whereas the milled Israel sample falls clearly below the other FF curves for all $T > 237\,K$. Of the intermediately active samples, the Taklamakan and Great Basin samples are at the upper end whereas the Dubai sample shows the second lowest FF values. The remaining samples are mostly not significantly different, with FF values lying within each others error bars.

The five Saharan samples in Fig. 4c cover a comparable range of FF to the non-Saharan ones at any temperature. The only surface-collected Saharan sample (Morocco) has higher FF values compared to the airborne Saharan samples. All

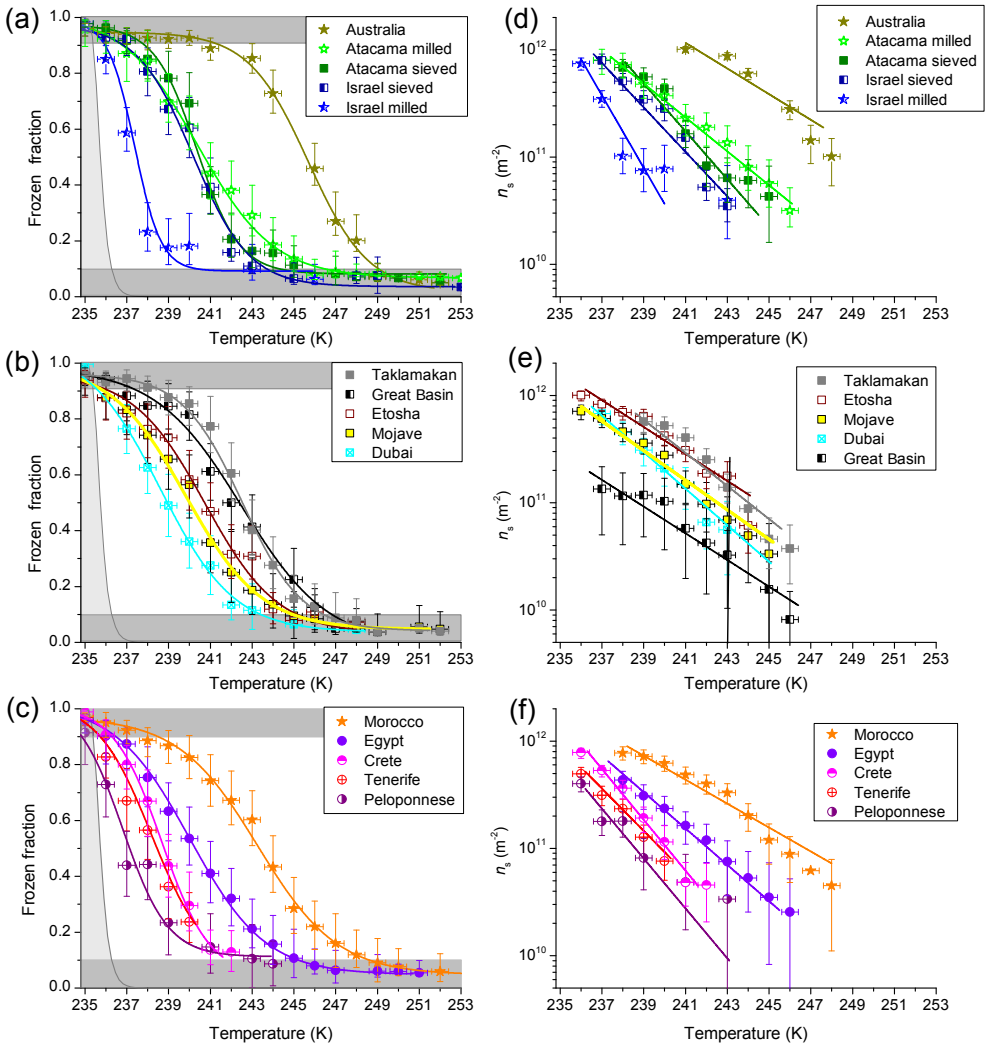

Figure 4. Frozen fraction of non-Saharan samples (panels **a** and **b**) and samples originating in the Sahara (panel **c**). Data were binned into 1 K-intervals. Lines are best sigmoidal fits. Squares are surface-collected and sieved; stars are surface-collected and milled; circles are airborne samples. The light gray area is the homogeneous freezing regime derived from classical nucleation theory (Hoyle et al., 2011; Ickes et al., 2015) and the two dark gray rectangles show the upper and lower detection limits of IODE. Ice-active surface site density of non-Saharan (panels **d** and **e**) and Saharan samples (**f**). Lines are best exponential fits to Eq. (6). The fit parameters are given in Table 4.

samples were fit with sigmoidal curves. None of the samples shows a stepwise FF owing to the polydisperse size distribution of the particles. Due to the heterogeneous particle composition, a partial step-like activation spectrum could be expected with decreasing temperature if the single mineral components were externally mixed and not present within one particle. Since ice nucleation activity is also dependent on the surface area of each particle (Archuleta et al., 2005; Connolly et al., 2009; Welti et al., 2009), larger particles will activate at higher temperatures than smaller ones, smoothing out the potential step function of different minerals.

n_s was calculated from the FF using $\overline{A_{ve,w}}$ in Eq. (3) to account for differences in the size distributions which may impact the ice nucleation behavior. The results are shown in the plots on the right side of Fig. 4. The error bars in n_s are derived by error propagation from the error in FF and $\delta(\overline{A_{ve,w}})$ and are dominated by the error in FF. Data points outside of $0.1 < FF < 0.9$ and in the homogeneous freezing regime are omitted. The n_s of the Australia sample remains the highest of all samples and that of the Israel milled sample one of the lowest. The n_s of the Great Basin sample, which has one of the highest FFs, is amongst the lowest due to its coarse particle sizes. Like their FF, the range of n_s of the Saharan samples is comparable to those of the non-Saharan ones (Fig. 4f). Among the Saharan samples, the n_s of the Tenerife sample is similar to that of Crete, whereas the Egypt sample is higher for $T > 238$ K. The n_s of the surface-collected and milled Morocco sample is distinctly higher at all temperatures.

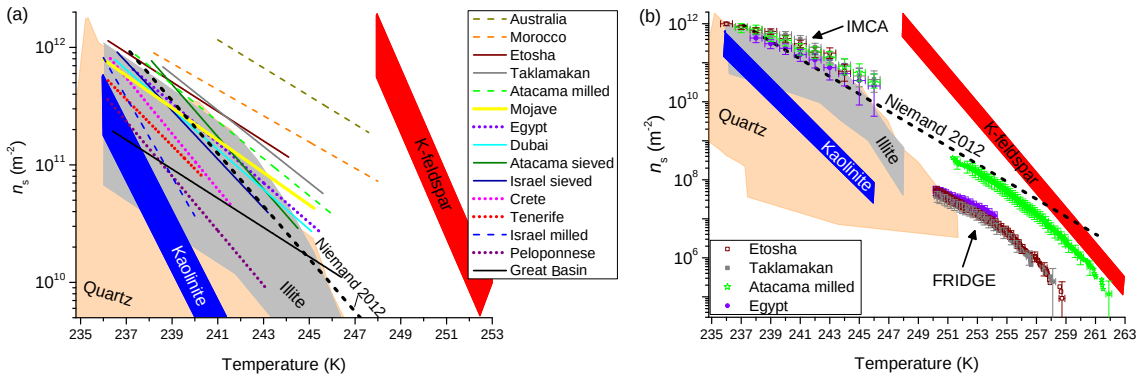

Figure 5. (a) Ice-active surface site density fits for all dust samples. The fit parameters are given in Table 4. Solid lines indicate surface-collected and sieved samples, dashed lines surface-collected, and milled samples and dotted lines are airborne samples. **(b)** Full temperature range measurements are taken by IMCA and FRIDGE. Colors and markers are the same as in Fig. 4. IMCA data are binned into 1 K-intervals. Error bars are drawn for every 10th data point. A parameterization for desert dust from Niemand et al. (2012) is shown as a thick dashed line. Parameterizations for kaolinite (Murray et al., 2011), illite (Broadley et al., 2012), and K-feldspar (Atkinson et al., 2013) as well as the range of data for quartz (Atkinson et al., 2013; Zolles et al., 2015) are given as areas representing the range between $n_{s,BET}$, as provided in the literature, and the corresponding $n_{s,geo}$. See text for details on the calculations of $n_{s,geo}$.

To compare all dust samples, the n_s in m^{-2} was fitted using the exponential function:

$$n_s = \exp(-a(T - 273.15\,\mathrm{K}) + b), \quad (6)$$

with the fit parameters a and b, which are given in Table 4 for each sample. The resulting fit lines from all samples are shown in Fig. 5a. Overall the Australia sample is by far the most ice nucleation-active sample. The Israel milled, Great Basin, and Peloponnese samples show a low ice nucleation activity. For comparison, the n_s fits for K-feldspar from Atkinson et al. (2013), for kaolinite KGb-1b from Murray et al. (2011), for Illite NX from Broadley et al. (2012), data for quartz from Atkinson et al. (2013) and Zolles et al. (2015), and the n_s parameterization curve from Niemand et al. (2012) are shown. The K-feldspar, kaolinite, illite, and quartz curves and data points were provided as $n_{s,BET}$, i.e., the surface area of the particles was measured with the Brunauer–Emmett–Teller (BET) nitrogen adsorption method (Brunauer et al., 1938). This method yields typically a higher surface area than that based on volume equivalent diameter. The literature $n_{s,BET}$ was converted to n_s using a conversion factor of 3.5 in case of K-feldspar as given in the Supplement of Atkinson et al. (2013). For illite, we followed Hiranuma et al. (2015), using a specific surface area (SSA) of 104.2 m^2 g^{-1} (Broadley et al., 2012) and a ratio of total surface area to total mass of 6.54 m^2 g^{-1} (Hiranuma et al., 2015). Similarly, for kaolinite we used SSA = 11.8 m^2 g^{-1}, a density of 2.63 g cm^{-3}, and a mean mass-weighted diameter of 674 nm (Hudson et al., 2008), yielding a correction factor of 3.49. For the same $n_{s,BET}$ values, the three quartz samples from Zolles et al. (2015) were active over a range of 10 K. No SSA values were provided and therefore we used also a conversion factor of 3.5 given that feldspar is somewhat similar to quartz. This comes with a very high uncertainty, as the size distribution and particle shape of quartz are likely to differ from the K-feldspar of Atkinson et al. (2013). The K-feldspar, kaolinite, illite, and quartz n_s areas cover the range from the $n_{s,BET}$ as provided in the literature and the calculated n_s to show the uncertainty inherent to the conversion. It can be seen that all desert dust samples fall between the K-feldspar and the clay mineral and quartz fits at all temperatures.

Similarly to our study the parameterization from Niemand et al. (2012) was based on the $n_s(T)$ of three polydisperse surface-collected dust samples from China, Egypt, and the Canary Islands and one sample collected after deposition in Israel. For $T < 250$ K the parameterization falls in the lower end of the range of n_s observed for our broader collection of global surface-collected and airborne dust samples (a factor of 3 to 4 below the average $n_s(T)$ of all measured curves; not shown). Given that the measurements were conducted with different instruments, which can lead to a systematic offset of up to 3 orders of magnitude in terms of n_s (Hiranuma et al., 2015), and the polydisperse size distribution of the dust samples, the agreement is considered reasonable. The maximum difference in temperature between the parameterization from Niemand et al. (2012) and the average of all n_s curves from this study (not shown) is less than 3 K, while the spread in n_s curves across all samples in our study is up to 10 K. The parameterization has a slope close to that of all airborne samples, whereas most of the surface-collected samples show a more moderate slope, i.e., a lower temperature dependence. This can be seen as an indication of active sites, which activate at warmer temperatures, being more frequent in the surface-collected samples compared to the airborne samples.

The high temperature measurements from FRIDGE for four samples are shown in Fig. 5b together with those from IMCA and parameterizations. Again, the desert dusts fall

between extrapolations of the clay mineral and K-feldspar fits. The parameterization from Niemand et al. (2012) predicts 1 to 2 orders of magnitude higher n_s than measured by FRIDGE. Only for the Atacama milled sample does the parameterization show about 30 % higher values than the measurements at $T = 251$–256 K. While at $T < 250$ K the n_s values of the four samples mostly overlap within error bars, at $T > 250$ K the Atacama milled sample has about 1 order of magnitude higher n_s than the other three samples. This shows that the fits of $n_s(T)$ are not constant over the whole temperature spectrum and are only valid for the given range. It indicates that the Atacama milled sample contains active sites at these temperatures which are missing in the other samples.

Figure 6a shows the median and minimum to maximum $n_s(T)$ range of the airborne and surface-collected samples. This illustrates that the n_s range of the airborne samples falls in the lower half of the n_s range of the surface-collected samples or even below. It shows that for immersion-mode ice nucleation, surface-collected dust samples are not representative for airborne dust samples, which all stem from North Africa, the world's largest source of atmospheric dust. This might be caused by a non-representative surface-dust collection, e.g., soil rather than dust is collected which has a different size distribution and composition, or dust from a location where threshold wind velocities for dust lifting are not reached. Another cause could be that atmospheric processes taking place during or after particle lofting may alter the particle surface and decrease the ice nucleation ability which has been suggested to occur in the field (Cziczo et al., 2013) and laboratory (Sullivan et al., 2010; Augustin-Bauditz et al., 2014). The potential effects of mineralogy on the ice nucleation activity at different temperatures is investigated in the following section.

3.3 Role of mineralogy

Various earlier studies have shown that the ice nucleation activity expressed by n_s varies by several orders of magnitude between different types of minerals. By analyzing the bulk mineralogy we investigate whether the dust's mineralogical composition explains the observed ice nucleation activity. Tables 2 and 3 show the results of the mineralogical analysis of the dust samples. The distinct composition of the Australia sample is striking, consisting almost entirely of quartz (91.3 wt %) and K-feldspars (4.2 wt % orthoclase, 3.9 wt % microcline), which are highly ice-active minerals in the immersion mode (Atkinson et al., 2013; Zolles et al., 2015). The Morocco sample also has a high quartz content (63.8 wt %), followed by the Taklamakan sample (33.1 wt %), both being two of the most ice-active samples of this study. The remaining samples have a quartz content of 23 wt % or less. Another obvious difference is the high feldspar content of both Atacama samples (milled: 22.3 wt % orthoclase, 43.2 wt % Na-plagioclase; sieved: 11.8 wt % orthoclase, 39.3 wt % Na-plagioclase). The milled Atacama sample shows the highest n_s of the four investigated samples in FRIDGE at $T > 250$ K (Fig. 5b), close to the K-feldspar parameterization by Atkinson et al. (2013) at $260 < T < 262$ K and also higher activities than the sieved sample at $T > 240$ K (Fig. 6b). The Israel samples have a distinctly high calcite content (milled: 81 wt %; sieved: 67.2 wt %), followed by Dubai (37.2 wt %) and Peloponnese (33 wt %). Calcite has been found to be a weakly ice-active mineral in the immersion mode (Atkinson et al., 2013; Zolles et al., 2015) and also in the condensation mode (Roberts and Hallett, 1969; Zimmermann et al., 2008). The Etosha sample consists of about one quarter each of calcite (29 wt %), dolomite (27 wt %), and ankerite (23 wt %) with 10 wt % muscovite and no significant fraction of clay minerals, feldspars, or quartz (1 wt % smectite and 1 wt % quartz were identified). This is surprising as the Etosha sample is one the most ice nucleation-active samples at $T < 242$ K. The ice nucleation ability of the mica muscovite is debated as some studies have found hardly any ice nucleation activity at heterogeneous freezing temperatures (Atkinson et al., 2013; Campbell et al., 2015; Kaufmann et al., 2016) while others found significant ice nucleation ability at $T < 243$ K (Steinke, 2013; Abdelmonem et al., 2015). Kaufmann et al. (2016) found little ice nucleation activity of a reference dolomite sample. Thus, the high ice nucleation activity at $T < 242$ K of the Etosha sample is not explainable by the known ice nucleation ability of its mineral components. To our knowledge, no study so far has investigated the ice nucleation behavior of pure ankerite.

The remaining samples are more complex mixtures of quartz, feldspars, clay minerals, micas, and other minerals. We find less than 4 wt % microcline in the sieved and milled Israel and the airborne Tenerife samples. In the samples from Australia and Morocco both K-feldspars orthoclase and microcline seem to be present. The surface-collected Great Basin sample contained 30 wt % microcline in the bulk sample but likely much less in the size fraction < 2.5 µm. The Sa-

Table 4. Overview of the dust n_s fit parameters a and b, the resulting R^2, and the number of data points in each fit, N.

Sample number	Collection site	Type	a (K^{-1})	b	R^2	N
1	Atacama	sieved	0.513	9.39	0.91	36
2	Atacama	milled	0.363	14.50	0.96	50
3	Australia	milled	0.274	18.93	0.89	16
4	Crete	airborne	0.545	7.32	0.98	30
5	Dubai	sieved	0.391	13.04	0.96	35
6	Egypt	airborne	0.390	13.22	0.96	41
7	Etosha	sieved	0.289	17.09	0.93	33
8	Great Basin	sieved	0.286	15.47	0.93	35
9	Israel	sieved	0.477	10.11	0.91	39
10	Israel	milled	0.777	−1.43	0.95	13
11	Mojave	sieved	0.317	15.62	0.96	46
12	Morocco	milled	0.257	18.55	0.95	45
13	Peloponnese	airborne	0.535	6.84	0.95	17
14	Taklamakan	sieved	0.355	15.00	0.93	21
15	Tenerife	airborne	0.455	10.16	0.97	14

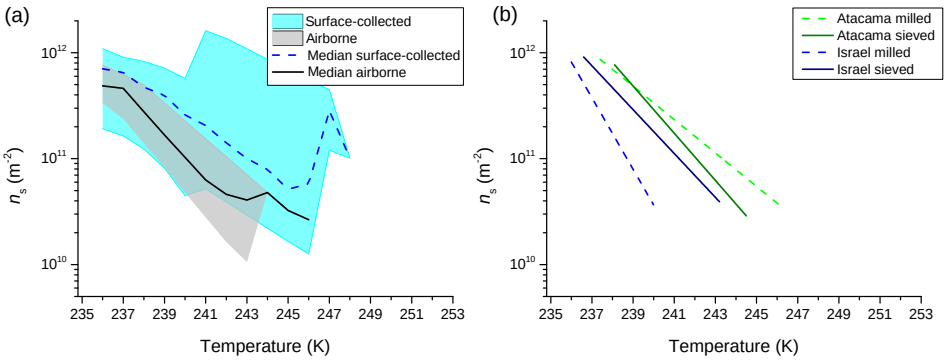

Figure 6. (a) Median and minimum to maximum n_s range of airborne and surface-collected samples. **(b)** Comparison of ice-active surface site density of milled and sieved samples.

haran samples show a great variety with the Tenerife sample having the highest content of clay minerals (illite + kaolinite + smectite + palygorskite: 57.7 wt %) of all dusts, similar to the findings of Alastuey et al. (2005). The other airborne Saharan samples (Egypt, Peloponnese, and Crete) consist to about 50 wt % of quartz and calcite, likely due to different source regions within the Sahara. The mineral fraction of the main minerals in soil samples is not homogeneous throughout the Sahara (Nickovic et al., 2012). Based on air mass back trajectory calculations the Tenerife sample originated in Northern Mauritania or Morocco, whereas the Egypt sample stemmed from local sources in Egypt and the Peloponnese and Crete samples from Northern Saharan sources in Algeria, Tunisia, and Libya. Schütz and Sebert (1987) found that the mineral composition of the size fraction < 5 µm of surface-collected samples in the Sahara was very similar throughout the Sahara and concluded that this size fraction is already well mixed within the desert. The main differences were a higher calcite and palygorskite content in the Northern Sahara, which is consistent with our findings for the Egypt, Peloponnese, and Crete samples in the case of calcite. We find comparable amounts of palygorskite in the Crete, Peloponnese, and Tenerife samples (4.5–5.3 wt %) but no palygorskite in the Egypt and Morocco samples. The differences with regard to mineralogical composition and ice nucleation ability found between the Morocco (higher quartz content) and Tenerife (higher clay mineral content) samples shows that, even if the source region of an airborne sample can be roughly localized, the mineralogy of surface-based and airborne samples can differ: surface-collected samples are not necessarily representative of the dust aerosol. This is supported by the fact that the Morocco sample consisted mostly of dust grains larger than 32 µm, which sediment quickly before being transported long distances in the atmosphere.

In the following we investigate if the different n_s values of the dust samples can be attributed to their mineralogy. For this, we compare the fraction of single minerals to the n_s of our dust samples at five different temperatures, using the most prominent minerals which have been found to have n_s values in a range which is measurable with IMCA-ZINC (Atkinson et al., 2013; Hiranuma et al., 2015; Zolles et al., 2015; Harrison et al., 2016; Peckhaus et al., 2016). Those are quartz, illite, kaolinite, and calcite. Additionally, we compare the samples' n_s to the following sums of minerals: K-feldspars (microcline plus orthoclase); all feldspars (K-feldspars plus Na-plagioclase feldspars); sum of all feldspars plus quartz; sum of all feldspars plus quartz plus illite and/or kaolinite. We do not differentiate between the different K-feldspar polymorphs because even the same type of feldspar can vary in n_s as shown by Harrison et al. (2016) due to the complex structure of feldspars. For each temperature, all samples which showed a FF between 0.1 and 0.9 were used for the correlations. The Etosha sample was excluded from the correlations with feldspars, quartz, and clays, as it does not contain any significant amount of these minerals. However, it was included for the comparison with calcite.

Table 5 shows the Pearson correlation coefficients (R) between the mineral fractions and the n_s at five temperatures. Only a few correlations are statistically significant, owing to the low number of samples. Nevertheless, the overview of the correlation coefficients gives an idea of the effect of certain minerals on n_s. The related scatter plots are given in Fig. 1 of the Supplement.

At 253 K only three samples (Atacama milled, Egypt, and Taklamakan) are available for comparison. For these, the K-feldspar content leads to a very high correlation ($R = 0.97$) and adding the Na-plagioclase to the feldspar sum reduces the R value to 0.87. At lower temperatures, no correlation is found between the K-feldspar content and n_s. At 245 K, the n_s correlates best ($R = 0.89$) with the quartz alone and adding feldspar, illite, or kaolinite leads to a lower R value (0.65–0.80). This is in agreement with earlier studies showing the comparable high immersion mode ice nucleation activity of some quartz samples at this temperature (Atkinson et al., 2013; Zolles et al., 2015). Interestingly, this behavior stays the same at 243 K ($R = 0.91$). At 240 and 238 K the quartz correlation is not as good and adding feldspars to the quartz improves the correlation (from $R = 0.52$ and 0.45 to

Table 5. Overview of the Pearson correlation coefficients of the sum of selected mineral fractions and $\ln(n_s)$ at different temperatures. The names of the included sample numbers can be found in Tables 1 and 4. At 253 K only four samples were measured. At $T \leq 245$ K only samples with FF between 0.1 and 0.9 were included for the correlations. The Etosha sample (7) was only included in the correlation with calcite because it does not contain feldspars, illite, or kaolinite and only traces of quartz. An asterisk indicates that the correlation was significant at the 0.05 level.

$\ln(n_s)$ at	253 K	245 K	243 K	240 K	238 K
Number of samples	3 (4)	7	11 (12)	13 (14)	13 (14)
Samples included	2, 6, (7), 14	2, 3, 6, 8, 11, 12, 14	1, 2, 3, 5, 6, (7), 8, 9, 11, 12, 13, 14	1, 2, 4, 5, 6, (7), 8, 9, 10, 11, 12, 13, 14, 15	
K-feldspar	0.97	−0.42	−0.13	0.05	−0.14
Feldspars	0.87	−0.29	−0.12	0.37	0.30
Quartz	−0.96	0.89*	0.91*	0.52*	0.45
Illite		−0.11	-0.39	−0.14	−0.16
Kaolinite	−0.35	−0.66	−0.47	−0.55	−0.61*
Feldspars + quartz	0.66	0.78*	0.77*	0.65*	0.54
Feldspars + quartz + illite	0.66	0.80*	0.73*	0.62*	0.51
Feldspars + quartz + kaolinite	0.74	0.65	0.69*	0.50	0.37
Feldspars + quartz + illite + kaolinite	0.74	0.68	0.64*	0.47	0.34
Calcite	−0.81	−0.58	−0.49	−0.45	−0.36

0.65 and 0.54, respectively). Note that the Australia sample, which has the highest quartz content, is excluded at 240 and 238 K from the correlation analysis because FF was > 0.9. Illite alone shows a weak negative correlation with n_s at any of the investigated temperatures and leads to reduced or constant R values when added to the quartz plus feldspar sum. Also calcite and kaolinite are negatively correlated with n_s at all presented temperatures. This means that a higher ice nucleation activity in one sample can be attributed at 253 K to the K-feldspar content present in this sample whereas at temperatures between 238 and 245 K it is attributed to the sum of feldspar and quartz content present. A high clay mineral content, in contrast, is associated with lower ice nucleation activity. To exclude a bias from varying numbers of samples at different temperatures, we have repeated the correlations at 245, 243, 240, and 238 K for the Atacama milled, Egypt, and Taklamakan samples only. The corresponding scatter plots are provided as Fig. 2 of the Supplement and confirm the observations that quartz plus feldspar yield the best correlations at $T < 245$ K.

These results need to be treated carefully, because the mineralogy is derived from the full size range up to 32 µm and may be different to the studied size fraction (< 2.5 µm). Therefore, we do the same analysis exclusively for the samples for which the size fraction larger than 2.5 µm was small and the mineralogical composition determined by XRD can be assumed to be representative for particles < 2.5 µm. These samples are the Atacama milled and sieved samples, the sieved Etosha, milled Israel and Australia, and the airborne Crete, Peloponnese, and Tenerife samples. From these samples only the ice nucleation ability of the Atacama milled and the Etosha sample was measured with FRIDGE at 253 K and only two of the samples show measurable n_s at 245 K in the IMCA data, and thus those temperatures are excluded. The results for 243, 240, and 238 K are given in Table 6. The correlation with illite and kaolinite is still negative at any temperature despite the fact that some of the samples in this subset contain a comparably large amount of these clay minerals (Tenerife: 21.8 wt %; Peloponnese: 20.2 wt %). At 243 K quartz shows the highest R value (0.91) for the selected samples. At 240 K and 238 K the sum of all feldspars ($R = 0.95$ and $R = 0.88$) and the sum of all feldspars plus quartz ($R = 0.97$ and $R = 0.90$) show the highest correlation with n_s. This is different to when all samples were included, where quartz exclusively led to the highest R values. The difference stems mainly from the exclusion of the Morocco, Taklamakan, Egypt, and Great Basin samples, which all had a high quartz content.

It should be noted that XRD is a bulk analysis of the mineralogical composition whereas ice nucleation is a process sensitive to the particle's surface, including cracks, crevices, or pores (Marcolli, 2014; Welti et al., 2014). Despite this difference in sensitivity, a high correlation between bulk mineralogy and ice nucleation activity is found in this study. As XRD does not allow any inference of the mixing state of different minerals it is not known, particularly for the small particles, if each particle contains some amount of quartz and/or feldspar or if pure calcite or clay mineral particles exist. However, our results indicate that feldspar or quartz present in the bulk dust will dominate its freezing behavior down to 238 K. While the correlations do not exclude an influence of non-mineral material, the results suggest that potential coatings or mixing of the particles only play a secondary role for the immersion freezing ability at the studied temperatures of the mineral dusts. The majority of the results can be explained by the mineralogy, as also observed by Kaufmann et al. (2016). This may be due to a significant dilution of coating material in the droplets forming on each dust particle and may have a more prominent role in deposition nucleation. Measurements in the condensation mode, which is the subject of Part 2 of this study, suggest that the

Table 6. Overview of the Pearson correlation coefficients of the sum of ice-active minerals and $\ln(n_s)$ at different temperatures of the samples where the mineralogy is representative for the size fraction smaller than 2.5 µm. The names of the included sample numbers can be found in Tables 1 and 4. Only samples with FF between 0.1 and 0.9 were included for the correlations. The Etosha sample (7) was only included in the correlation with calcite because it does not contain feldspars, illite, or kaolinite and only traces of quartz. An asterisk indicates if the correlation was significant at the 0.05 level.

$\ln(n_s)$ at	243 K	240 K	238 K
Number of samples	4 (5)	6 (7)	6 (7)
Samples included	1, 2, 3, (7), 13	1, 2, 4, (7), 10, 13, 15	
K-feldspar	0.04	0.89*	0.79
All feldspars	−0.30	0.95*	0.88*
Quartz	0.91	0.09	0.12
Illite	−0.80	−0.05	−0.17
Kaolinite	−0.56	−0.40	−0.36
Feldspars + quartz	0.87	0.97*	0.90*
Feldspars + quartz + illite	0.84	0.93*	0.84*
Feldspars + quartz + kaolinite	0.90	0.95*	0.88*
Feldspars + quartz + illite + kaolinite	0.87	0.90*	0.82*
Calcite	−0.45	−0.64	−0.61

ice nucleation activity of this sample is in large part related to organic or biological material mixed with the dust.

3.4 Effect of milling

Two of the dust samples have undergone two different treatments (sieving and milling) to compare the effect of milling on n_s of a polymineral sample. The Israel sample was first sieved and then part of the $d \leq 32$ µm fraction was milled. For the Atacama sample, the original sample containing particles of all sizes was split: one part was sieved and one part milled. The resulting n_s curves are shown in Fig. 6b. Interestingly, the two sieved samples are very similar in n_s. The milling of the Atacama sample led to a slightly higher ice nucleation efficiency at $T > 240$ K compared to the sieved sample. Contrastingly, for the Israel sample milling led to a decrease in n_s at all studied temperatures above 237 K. The latter could be related to the high calcite content of the Israel dust. Calcite is a rather soft mineral with a Mohs hardness of 3 and a perfect cleavage, and during the milling process it could be ground to a smaller grain size faster than compared to harder minerals such as quartz (Mohs hardness of 7) or feldspar (6). Thus the size fraction $d_{ve} \leq 2.5$ µm (the D_{50} cutoff of the particle generation system used) could be enriched in calcite. Calcite has been found to be ice-active only very close to the homogeneous freezing regime (Atkinson et al., 2013; Zolles et al., 2015) and negatively correlated with n_s at all presented temperatures in this study (Tables 5 and 6). Similarly, the slightly higher n_s at $T > 240$ K of the milled Atacama sample is likely due to more feldspar being present in the $d_{ve} > 32$ µm fraction compared to the sieved sample, which then got milled into sizes $d_{ve} < 2.5$ µm. It can be seen from Tables 2 and 3 that the K-feldspar (orthoclase) content is higher in the Atacama milled sample (22 wt %) than in the sieved one (12 wt %). The milled sample mostly consisted of particles smaller than 2.5 µm, whereas the sieved one had a large fraction of particles larger than 2.5 µm. Thus, there was likely more orthoclase content in the milled Atacama sample particles smaller than 2.5 µm compared to those in the sieved sample, leading to higher n_s at warmer temperatures. Effects such as an increase in surface irregularities, defect density, and functional groups due to the milling as reported by other authors (Hiranuma et al., 2014; Zolles et al., 2015) are not excluded but were not investigated in this study. An increase in defect density and surface irregularities has been shown to increase the ice nucleation activity of monomineral or single compound samples. As milling reduced the ice nucleation activity of the Israel sample, we conclude for this specific sample that any morphology effect is small in comparison to the change in mineralogical composition of the analyzed size range caused by the milling. This emphasizes the importance of mineralogy for the surface sensitive ice nucleation process.

4 Conclusions

The ice nucleation ability in the immersion mode of 15 natural desert dust samples was quantified by the frozen fraction and ice-active surface site density and compared with the bulk dust mineralogy. A diverse mineralogical composition was found for the different desert dust samples which can be related to variable ice nucleation abilities. The comparison showed that at temperatures above 250 K the highest n_s is related to the highest K-feldspar content in the sample confirming earlier findings on the superior ice nucleation ability of K-feldspars compared to other minerals. Microcline was found in one airborne sample (4 wt %) and in surface-collected samples from four different locations. We could not confirm a superior role of microcline over orthoclase, in

part because a differentiation of the two minerals was often difficult and partly because their content was too low in the size range investigated for ice nucleation to cause an effect detectable with the IMCA-ZINC experiment. A conclusion on the atmospheric relevancy of microcline is therefore not possible because even in low amounts – of a few percent – it could nucleate ice and glaciate clouds at temperatures warmer than 253 K.

At temperatures below 250 K, the ice nucleation ability was mainly attributed to the quartz content of the samples, as well as to the sum of all feldspars (K-feldspars and Na-plagioclase feldspars). Keeping in mind that quartz is ubiquitous in atmospheric desert dust, this suggests that quartz plays a more prominent role for atmospheric ice nucleation than previously thought. The clay mineral (illite and kaolinite) and calcite content of the dust samples negatively correlated with n_s at all studied temperatures, suggesting a minor importance of these minerals for the ice nucleation activity of natural dust samples in the immersion mode, especially if quartz or feldspar are present. Atkinson et al. (2013) suggested that the global mineral dust INP concentration down to a temperature of about 240 K is dominated by feldspar. At temperatures between the homogeneous freezing limit and 240 K, where quartz is an active INP, it dominates the total INP concentration as it is much more abundant than feldspar. Our experiments on natural dust confirm this suggestion.

The variation in mineralogy with particle size leads to variations in n_s. The most ice nucleation-active mineral feldspar is less common in the smallest dust size fractions. Quartz is found in all size ranges but more common in the larger dust size fractions. The less ice nucleation-active clay minerals and calcite dominate the small size fraction. As the size distribution of dust changes during atmospheric transport, a resulting change in mineralogy will have implications for the atmospheric relevance of certain mineral components. Three of the four airborne samples (Crete, Peloponnese, and Tenerife) had the highest clay mineral content and were amongst the least ice nucleation-active samples. For all desert dust samples we found a high correlation of the ice nucleation activity of particles smaller than 2.5 µm with the quartz content of the dust samples. This shows that despite the dominance of the clay minerals in the small size fraction, quartz is an important atmospheric INP component and also found in the particle size fraction with the longest atmospheric residence time.

Milling of dust samples in the laboratory or by natural mechanical weathering processes can lead to more surface inhomogeneities and also to an enrichment of more ice nucleation-active minerals, such as quartz, in sizes relevant for atmospheric ice nucleation. This potentially explains the higher ice nucleation activity of Arizona test dust compared to desert dust samples found in earlier studies (Zolles et al., 2015; Kaufmann et al., 2016). The observed differences between the surface-collected and the airborne Saharan dust samples suggest that surface-collected dust may not be representative of atmospheric dust transported over long distances. Thus, more ice nucleation studies on airborne, transported dust also from deserts other than the Sahara are crucial to quantify the ability of atmospheric dust to nucleate ice. Furthermore, if airborne dust is generally found to be less ice nucleation active than surface-collected dust and does not show ice nucleation activity at temperatures above 263 K, it cannot explain first ice formation in clouds with top temperatures warmer than 263 K. For that other INP such as biological particles or different mechanisms such as seeder – feeder processes would need to be investigated. In our study the ice nucleation activity of only one sample (Etosha) was not explainable by the known ice nucleation activity of its mineral components. The role of adsorbed organic material for the ice nucleation activity of the dust samples will be investigated in Part 2 of this paper series.

The applicability of the parameterization by Niemand et al. (2012) to describe an average ice nucleation behavior of desert dust was confirmed by a global set of dust samples. However, the variation between the different samples in temperature was up to 10 K. To more adequately describe immersion freezing by desert dust in the atmosphere, mineralogy sensitive emission and transport schemes would be desirable. We suggest that K-feldspar for temperatures above 250 K and for lower temperatures additionally Na-plagioclase feldspars and quartz emissions and transport should be quantified. Since this is complex and computationally expensive to implement, more studies quantifying the ice nucleation ability of dust as it is found in the atmosphere may circumvent this complexity.

5 Data availability

The ice nucleation data shown in Fig. 4 and the data used for the correlation coefficient analysis are uploaded at https://polybox.ethz.ch/index.php/s/CU6iHJR0ITGFpcb (Boose and Kanji, 2016). Other data can be obtained from the corresponding authors.

The Supplement related to this article is available online at doi:10.5194/acp-16-15075-2016-supplement.

Author contributions. Y. Boose collected the Tenerife and Israel samples, initiated, planned, and led the measurements, performed and analyzed the XRD measurements, analyzed the INP and aerosol data and wrote the manuscript, A. Welti, J. Atkinson, and F. Ramelli conducted the IMCA measurements, A. Welti analyzed the IMCA data and collected the Australia, Mojave, and Great Basin sample, A. Danielczok performed the FRIDGE sample collection and analysis, H. G. Bingemer supervised the FRIDGE data analysis and contributed to the manuscript, M. Plötze performed and analyzed the XRD measurements, and B. Sierau, Z. A. Kanji, and U. Lohmann supervised the project and contributed to the manuscript.

Acknowledgements. The various dust samples in this paper have been collected by a number of people to whom the authors are very thankful: Maria Kanakidou and her team (Peloponnese, Crete), Felix Lüönd (Atacama), Paolo D'Odorico and Christopher Hoyle (Etosha), Lukas Kaufmann, Konrad Kandler and Lother Schütz (Taklamakan), Monika Kohn (Dubai), Joel Corbin (Morocco), Sergio Rodríguez (Tenerife), and Hamza Mohamed Hamza (Egypt). Furthermore, we thank the rest of campaign members: Annika Kube, Larissa Lacher, and Fabian Mahrt, as well as Hannes Wydler for technical support. Y. Boose is funded by the Swiss National Science Foundation (grant 200020 150169/1). The research leading to these results has received funding from the European Union's Seventh Framework Programme (FP7/2007-797 2013) under grant agreement no. 603445 (BACCHUS). A. Danielczok and H. G. Bingemer gratefully acknowledge support by Deutsche Forschungsgemeinschaft (DFG) under the Research Unit FOR 1525 (INUIT).

Edited by: H. Grothe
Reviewed by: T. Zolles and one anonymous referee

References

Abdelmonem, A., Lützenkirchen, J., and Leisner, T.: Probing ice-nucleation processes on the molecular level using second harmonic generation spectroscopy, Atmos. Meas. Tech., 8, 3519–3526, doi:10.5194/amt-8-3519-2015, 2015.

Alastuey, A., Querol, X., Castillo, S., Escudero, M., Avila, A., Cuevas, E., Torres, C., Romero, P.-M., Exposito, F., García, Diaz, J., Van Dingenen, R., and Putaud, J. P.: Characterisation of TSP and $PM_{2.5}$ at Izaña and Sta. Cruz de Tenerife (Canary Islands, Spain) during a Saharan Dust Episode (July 2002) , Atmos. Environ., 39, 4715–4728, doi:10.1016/j.atmosenv.2005.04.018, 2005.

Alexander, J. M.: Optical properties of mineral dust aerosol including analysis of particle size, composition, and shape effects, and the impact of physical and chemical processing, PhD thesis, University of Iowa, 2015.

Archuleta, C. M., DeMott, P. J., and Kreidenweis, S. M.: Ice nucleation by surrogates for atmospheric mineral dust and mineral dust/sulfate particles at cirrus temperatures, Atmos. Chem. Phys., 5, 2617–2634, doi:10.5194/acp-5-2617-2005, 2005.

Ardon-Dryer, K. and Levin, Z.: Ground-based measurements of immersion freezing in the eastern Mediterranean, Atmos. Chem. Phys., 14, 5217–5231, doi:10.5194/acp-14-5217-2014, 2014.

Atkinson, J., Murray, B. J., Woodhouse, M. T., Whale, T. F., Baustian, K. J., Carslaw, K. S., Dobbie, S., O'Sullivan, D., and Malkin, T. L.: The importance of feldspar for ice nucleation by mineral dust in mixed-phase clouds, Nature, 498, 355–358, doi:10.1038/nature12278, 2013.

Augustin-Bauditz, S., Wex, H., Kanter, S., Ebert, M., Niedermeier, D., Stolz, F., Prager, A., and Stratmann, F.: The immersion mode ice nucleation behavior of mineral dusts: A comparison of different pure and surface modified dusts, Geophys. Res. Lett., 41, 1–8, doi:10.1002/2014GL061317, 2014.

Avila, A., Queralt-Mitjans, I., and Alarcón, M.: Mineralogical composition of African dust delivered by red rains over northeastern Spain, J. Geophys. Res. Atmos., 102, 21977–21996, doi:10.1029/97JD00485, 1997.

Bergmann, J., Friedel, P., and Kleeberg, R.: BGMN – a new fundamental parameters based Rietveld program for laboratory X-ray sources, its use in quantitative analysis and structure investigations, Commission of Powder Diffraction, International Union of Crystallography CPD Newslett., 20, 5–8, 1998.

Bish, D. L. and Plötze, M.: X-ray powder diffraction with emphasis on qualitative and quantitative analysis in industrial mineralogy, in: Industrial Mineralogy, EMU Notes in Mineralogy, edited by: Christidis, G., vol. 9, chap. 3, 35–76, 2011.

Boose, Y. and Kanji, Z. A.: Ice nuceation and mineralogy data set of desert dust samples, available at: https://polybox.ethz.ch/index.php/s/AjQknR3cQGVwVGU, last access: 11 November 2016.

Boose, Y., Kanji, Z. A., Kohn, M., Sierau, B., Zipori, A., Crawford, I., Lloyd, G., Bukowiecki, N., Herrmann, E., Kupiszewski, P., Steinbacher, M., and Lohmann, U.: Ice Nucleating Particle Measurements at 241 K during Winter Months at 3580 MSL in the Swiss Alps, J. Atmos. Sci., 73, 2203–2228, doi:10.1175/JAS-D-15-0236.1, 2016a.

Boose, Y., Sierau, B., García, M. I., Rodríguez, S., Alastuey, A., Linke, C., Schnaiter, M., Kupiszewski, P., Kanji, Z. A., and Lohmann, U.: Ice nucleating particles in the Saharan Air Layer, Atmos. Chem. Phys., 16, 9067–9087, doi:10.5194/acp-16-9067-2016, 2016b.

Boucher, O., Randall, D., Artaxo, P., Bretherton, C., Feingold, G., Forster, P., Kerminen, V.-M., Kondo, Y., Liao, H., Lohmann, U., Rasch, P., Satheesh, S., Sherwood, S., Stevens, B., and Zhang, X.: Clouds and Aerosols, in: Climate Change 2013: The Physical Science Basis, Contribution of Working Group I to the Fifth Assessment Report of the Intergovernmental Panel on Climate Change, edited by: Stocker, T. F., Qin, D., Plattner, G.-K., Tignor, M., Allen, S. K., Boschung, J., Nauels, A., Xia, Y., Bex, V., and Midgley, P. M., Cambridge University Press, Cambridge, United Kingdom and New York, NY, USA, 2013.

Broadley, S. L., Murray, B. J., Herbert, R. J., Atkinson, J. D., Dobbie, S., Malkin, T. L., Condliffe, E., and Neve, L.: Immersion mode heterogeneous ice nucleation by an illite rich powder representative of atmospheric mineral dust, Atmos. Chem. Phys., 12, 287–307, doi:10.5194/acp-12-287-2012, 2012.

Brooks, S. D., Suter, K., and Olivarez, L.: Effects of Chemical Aging on the Ice Nucleation Activity of Soot and Polycyclic Aromatic Hydrocarbon Aerosols, J. Phys. Chem. A, 118, 10036–10047, doi:10.1021/jp508809y, 2014.

Brunauer, S., Emmett, P. H., and Teller, E.: Adsorption of Gases in Multimolecular Layers, J. Am. Chem. Soc., 60, 309–319, doi:10.1021/ja01269a023, 1938.

Campbell, J. M., Meldrum, F. C., and Christenson, H. K.: Is Ice Nucleation from Supercooled Water Insensitive to Surface Roughness?, J. Phys. Chem. C, 119, 1164–1169, doi:10.1021/jp5113729, 2015.

Caquineau, S., Gaudichet, A., Gomes, L., Magonthier, M.-C., and Chatenet, B.: Saharan dust: Clay ratio as a relevant tracer to assess the origin of soil-derived aerosols, Geophys. Res. Lett., 25, 983–986, doi:10.1029/98GL00569, 1998.

Chou, C., Stetzer, O., Weingartner, E., Jurányi, Z., Kanji, Z. A., and Lohmann, U.: Ice nuclei properties within a Saharan dust event at the Jungfraujoch in the Swiss Alps, Atmos. Chem. Phys., 11, 4725–4738, doi:10.5194/acp-11-4725-2011, 2011.

Conen, F., Morris, C. E., Leifeld, J., Yakutin, M. V., and Alewell, C.: Biological residues define the ice nucleation properties of soil

dust, Atmos. Chem. Phys., 11, 9643–9648, doi:10.5194/acp-11-9643-2011, 2011.

Connolly, P. J., Möhler, O., Field, P. R., Saathoff, H., Burgess, R., Choularton, T., and Gallagher, M.: Studies of heterogeneous freezing by three different desert dust samples, Atmos. Chem. Phys., 9, 2805–2824, doi:10.5194/acp-9-2805-2009, 2009.

Cziczo, D. J., Froyd, K. D., Hoose, C., Jensen, E. J., Diao, M., Zondlo, M. A., Smith, J. B., Twohy, C. H., and Murphy, D. M.: Clarifying the Dominant Sources and Mechanisms of Cirrus Cloud Formation, Science, 340, 1320–1324, doi:10.1126/science.1234145, 2013.

Dall'Osto, M., Harrison, R. M., Highwood, E. J., O'Dowd, C., Ceburnis, D., Querol, X., and Achterberg, E. P.: Variation of the mixing state of Saharan dust particles with atmospheric transport, Atmos. Environ., 44, 3135–3146, doi:10.1016/j.atmosenv.2010.05.030, 2010.

D'Almeida, G. A. and Schütz, L.: Number, Mass and Volume Distributions of Mineral Aerosol and Soils of the Sahara, J. Clim. Appl. Meteorol., 22, 233–243, doi:10.1175/1520-0450(1983)022<0233:NMAVDO>2.0.CO;2, 1983.

DeMott, P. J.: An Exploratory Study of Ice Nucleation by Soot Aerosols, J. Appl. Meteorol., 29, 1072–1079, doi:10.1175/1520-0450(1990)029<1072:AESOIN>2.0.CO;2, 1990.

DeMott, P. J., Sassen, K., Poellot, M., Baumgardner, D., Rogers, D., Brooks, S., Prenni, A., and Kreidenweis, S.: African dust aerosols as atmospheric ice nuclei, Geophys. Res. Lett., 30, 1732, doi:10.1029/2003GL017410, 2003.

DeMott, P. J., Prenni, A. J., Liu, X., Kreidenweis, S. M., Petters, M. D., Twohy, C. H., Richardson, M. S., Eidhammer, T., and Rogers, D. C.: Predicting global atmospheric ice nuclei distributions and their impacts on climate, Proc. Natl. Acad. Sci. USA, 107, 11217–11222, doi:10.1073/pnas.0910818107, 2010.

DeMott, P. J., Hill, T. C. J., McCluskey, C. S., Prather, K. A., Collins, D. B., Sullivan, R. C., Ruppel, M. J., Mason, R. H., Irish, V. E., Lee, T., Hwang, C. Y., Rhee, T. S., Snider, J. R., McMeeking, G. R., Dhaniyala, S., Lewis, E. R., Wentzell, J. J. B., Abbatt, J., Lee, C., Sultana, C. M., Ault, A. P., Axson, J. L., Diaz Martinez, M., Venero, I., Santos-Figueroa, G., Stokes, M. D., Deane, G. B., Mayol-Bracero, O. L., Grassian, V. H., Bertram, T. H., Bertram, A. K., Moffett, B. F., and Franc, G. D.: Sea spray aerosol as a unique source of ice nucleating particles, Proc. Natl. Acad. Sci. USA, 113, 5797–5803, doi:10.1073/pnas.1514034112, 2015a.

DeMott, P. J., Prenni, A. J., McMeeking, G. R., Sullivan, R. C., Petters, M. D., Tobo, Y., Niemand, M., Möhler, O., Snider, J. R., Wang, Z., and Kreidenweis, S. M.: Integrating laboratory and field data to quantify the immersion freezing ice nucleation activity of mineral dust particles, Atmos. Chem. Phys., 15, 393–409, doi:10.5194/acp-15-393-2015, 2015b.

Falkovich, A. H., Ganor, E., Levin, Z., Formenti, P., and Rudich, Y.: Chemical and mineralogical analysis of individual mineral dust particles, J. Geophys. Res.-Atmos., 106, 18029, doi:10.1029/2000JD900430, 2001.

Harrison, A. D., Whale, T. F., Carpenter, M. A., Holden, M. A., Neve, L., O'Sullivan, D., Vergara Temprado, J., and Murray, B. J.: Not all feldspars are equal: a survey of ice nucleating properties across the feldspar group of minerals, Atmos. Chem. Phys., 16, 10927–10940, doi:10.5194/acp-16-10927-2016, 2016.

Hinds, W.: Aerosol Technology Properties, Behavior, and Measurement of Airborne Particles, 2nd Edn., John Wiley & Sons, Inc., 1999.

Hiranuma, N., Hoffmann, N., Kiselev, A., Dreyer, A., Zhang, K., Kulkarni, G., Koop, T., and Möhler, O.: Influence of surface morphology on the immersion mode ice nucleation efficiency of hematite particles, Atmos. Chem. Phys., 14, 2315–2324, doi:10.5194/acp-14-2315-2014, 2014.

Hiranuma, N., Augustin-Bauditz, S., Bingemer, H., Budke, C., Curtius, J., Danielczok, A., Diehl, K., Dreischmeier, K., Ebert, M., Frank, F., Hoffmann, N., Kandler, K., Kiselev, A., Koop, T., Leisner, T., Möhler, O., Nillius, B., Peckhaus, A., Rose, D., Weinbruch, S., Wex, H., Boose, Y., DeMott, P. J., Hader, J. D., Hill, T. C. J., Kanji, Z. A., Kulkarni, G., Levin, E. J. T., McCluskey, C. S., Murakami, M., Murray, B. J., Niedermeier, D., Petters, M. D., O'Sullivan, D., Saito, A., Schill, G. P., Tajiri, T., Tolbert, M. A., Welti, A., Whale, T. F., Wright, T. P., and Yamashita, K.: A comprehensive laboratory study on the immersion freezing behavior of illite NX particles: a comparison of 17 ice nucleation measurement techniques, Atmos. Chem. Phys., 15, 2489–2518, doi:10.5194/acp-15-2489-2015, 2015.

Hobbs, P. V. and Rangno, A. L.: Ice Particle Concentrations in Clouds, J. Atmos. Sci., 42, 2523–2549, doi:10.1175/1520-0469(1985)042<2523:IPCIC>2.0.CO;2, 1985.

Hoffer, T. E.: A laboratory investigation of droplet freezing, J. Meteorol., 18, 766–778, doi:10.1175/1520-0469(1961)018<0766:ALIODF>2.0.CO;2, 1961.

Hoose, C. and Möhler, O.: Heterogeneous ice nucleation on atmospheric aerosols: a review of results from laboratory experiments, Atmos. Chem. Phys., 12, 9817–9854, doi:10.5194/acp-12-9817-2012, 2012.

Hoyle, C. R., Pinti, V., Welti, A., Zobrist, B., Marcolli, C., Luo, B., Höskuldsson, Á., Mattsson, H. B., Stetzer, O., Thorsteinsson, T., Larsen, G., and Peter, T.: Ice nucleation properties of volcanic ash from Eyjafjallajökull, Atmos. Chem. Phys., 11, 9911–9926, doi:10.5194/acp-11-9911-2011, 2011.

Hudson, P. K., Gibson, E. R., Young, M. A., Kleiber, P. D., and Grassian, V. H.: Coupled infrared extinction and size distribution measurements for several clay components of mineral dust aerosol, J. Geophys. Res.-Atmos., 113, D01201, doi:10.1029/2007JD008791, 2008.

Ickes, L., Welti, A., Hoose, C., and Lohmann, U.: Classical nucleation theory of homogeneous freezing of water: thermodynamic and kinetic parameters, Phys. Chem. Chem. Phys., 17, 5514–5537, doi:10.1039/C4CP04184D, 2015.

Ignatius, K., Kristensen, T. B., Järvinen, E., Nichman, L., Fuchs, C., Gordon, H., Herenz, P., Hoyle, C. R., Duplissy, J., Garimella, S., Dias, A., Frege, C., Höppel, N., Tröstl, J., Wagner, R., Yan, C., Amorim, A., Baltensperger, U., Curtius, J., Donahue, N. M., Gallagher, M. W., Kirkby, J., Kulmala, M., Möhler, O., Saathoff, H., Schnaiter, M., Tomé, A., Virtanen, A., Worsnop, D., and Stratmann, F.: Heterogeneous ice nucleation of viscous secondary organic aerosol produced from ozonolysis of α-pinene, Atmos. Chem. Phys., 16, 6495–6509, doi:10.5194/acp-16-6495-2016, 2016.

Isono, K.: On ice-crystal nuclei and other substances found in snow crystals, J. Meteorol., 12, 456–462, doi:10.1175/1520-0469(1955)012<0456:OICNAO>2.0.CO;2, 1955.

Kandler, K., Benker, N., Bundke, U., Cuevas, E., Ebert, M., Knippertz, P., Rodríguez, S., Schütz, L., and Weinbruch, S.: Chemical composition and complex refractive index of Saharan Mineral Dust at Izaña, Tenerife (Spain) derived by electron microscopy, Atmos. Environ., 41, 8058–8074, doi:10.1016/j.atmosenv.2007.06.047, 2007.

Kandler, K., Schütz, L., Deutscher, C., Ebert, M., Hofmann, H., Jäckl, S., Jaenicke, R., Knippertz, P., Lieke, K., Massling, A., and et al.: Size distribution, mass concentration, chemical and mineralogical composition and derived optical parameters of the boundary layer aerosol at Tinfou, Morocco, during SAMUM 2006, Tellus B, 61, 32–50, doi:10.1111/j.1600-0889.2008.00385.x, 2009.

Kanji, Z. and Abbatt, J.: Ice nucleation onto Arizona Test Dust at cirrus temperatures: Effect of temperature and aerosol size on onset relative humidity, J. Phys. Chem. A., 114, 935–941, doi:10.1021/jp908661m, 2010.

Kanji, Z. A., DeMott, P. J., Möhler, O., and Abbatt, J. P. D.: Results from the University of Toronto continuous flow diffusion chamber at ICIS 2007: instrument intercomparison and ice onsets for different aerosol types, Atmos. Chem. Phys., 11, 31–41, doi:10.5194/acp-11-31-2011, 2011.

Kanji, Z. A., Welti, A., Chou, C., Stetzer, O., and Lohmann, U.: Laboratory studies of immersion and deposition mode ice nucleation of ozone aged mineral dust particles, Atmos. Chem. Phys., 13, 9097–9118, doi:10.5194/acp-13-9097-2013, 2013.

Kaufmann, L., Marcolli, C., Hofer, J., Pinti, V., Hoyle, C. R., and Peter, T.: Ice nucleation efficiency of natural dust samples in the immersion mode, Atmos. Chem. Phys., 16, 11177–11206, doi:10.5194/acp-16-11177-2016, 2016.

Knippertz, P. and Stuut, J.-B. W. (Eds.): Mineral Dust: A Key Player in the Earth System, Springer Dordrecht Heidelberg New York London, doi:10.1007/978-94-017-8978-3, 2014.

Knopf, D. A., Alpert, P. A., Wang, B., and Aller, J. Y.: Stimulation of ice nucleation by marine diatoms, Nat. Geosci., 4, 88–90, doi:10.1038/ngeo1037, 2011.

Knopf, D. A., Alpert, P. A., Wang, B., O'Brien, R. E., Kelly, S. T., Laskin, A., Gilles, M. K., and Moffet, R. C.: Microspectroscopic imaging and characterization of individually identified ice nucleating particles from a case field study, J. Geophys. Res.-Atmos., 119, 10365–10381, doi:10.1002/2014JD021866, 2014.

Krog, J. O., Zachariassen, K. E., Larsen, B., and Smidsrod, O.: Thermal buffering in Afro-alpine plants due to nucleating agent-induced water freezing, Nature, 282, 300–301, doi:10.1038/282300a0, 1979.

Kulkarni, G., China, S., Liu, S., Nandasiri, M., Sharma, N., Wilson, J., Aiken, A. C., Chand, D., Laskin, A., Mazzoleni, C., Pekour, M., Shilling, J., Shutthanandan, V., Zelenyuk, A., and Zaveri, R. A.: Ice nucleation activity of diesel soot particles at cirrus relevant temperature conditions: Effects of hydration, secondary organics coating, soot morphology, and coagulation, Geophys. Res. Lett., 43, 3580–3588, doi:10.1002/2016GL068707, 2016.

Kumai, M.: Identification of Nuclei and Concentrations of Chemical Species in Snow Crystals Sampled at the South Pole, J. Atmos. Sci., 33, 833–841, doi:10.1175/1520-0469(1976)033<0833:IONACO>2.0.CO;2, 1976.

Ladino, L. A., Zhou, S., Yakobi-Hancock, J. D., Aljawhary, D., and Abbatt, J. P. D.: Factors controlling the ice nucleating abilities of α-pinene SOA particles, J. Geophys. Res.-Atmos., 119, 9041–9051, doi:10.1002/2014JD021578, 2014.

Langham, E. J. and Mason, B. J.: The Heterogeneous and Homogeneous Nucleation of Supercooled Water, P. R. Soc. A, 247, 493–504, doi:10.1098/rspa.1958.0207, 1958.

Leinen, M., Prospero, J. M., Arnold, E., and Blank, M.: Mineralogy of aeolian dust reaching the North Pacific Ocean: 1. Sampling and analysis, J. Geophys. Res.-Atmos., 99, 21017–21023, doi:10.1029/94JD01735, 1994.

Lohmann, U. and Feichter, J.: Global indirect aerosol effects: a review, Atmos. Chem. Phys., 5, 715–737, doi:10.5194/acp-5-715-2005, 2005.

Lüönd, F., Stetzer, O., Welti, A., and Lohmann, U.: Experimental study on the ice nucleation ability of size-selected kaolinite particles in the immersion mode, J. Geophys. Res.-Atmos., 115, 1–14, doi:10.1029/2009JD012959, 2010.

Marcolli, C.: Deposition nucleation viewed as homogeneous or immersion freezing in pores and cavities, Atmos. Chem. Phys., 14, 2071–2104, doi:10.5194/acp-14-2071-2014, 2014.

Mason, B. J. and Ludlam, F. H.: The microphysics of clouds, Rep. Prog. Phys., 14, 147–195, 1950.

Meola, M., Lazzaro, A., and Zeyer, J.: Bacterial composition and survival on Sahara dust particles transported to the European Alps, Front. Microbiol., 6, 1454, doi:10.3389/fmicb.2015.01454, 2015.

Möhler, O., Field, P. R., Connolly, P., Benz, S., Saathoff, H., Schnaiter, M., Wagner, R., Cotton, R., Krämer, M., Mangold, A., and Heymsfield, A. J.: Efficiency of the deposition mode ice nucleation on mineral dust particles, Atmos. Chem. Phys., 6, 3007–3021, doi:10.5194/acp-6-3007-2006, 2006.

Möhler, O., Benz, S., Saathoff, H., Schnaiter, M., Wagner, R., Schneider, J., Walter, S., Ebert, V., and Wagner, S.: The effect of organic coating on the heterogeneous ice nucleation efficiency of mineral dust aerosols, Environ. Res. Lett., 3, 025007, doi:10.1088/1748-9326/3/2/025007, 2008a.

Möhler, O., Georgakopoulos, D. G., Morris, C. E., Benz, S., Ebert, V., Hunsmann, S., Saathoff, H., Schnaiter, M., and Wagner, R.: Heterogeneous ice nucleation activity of bacteria: new laboratory experiments at simulated cloud conditions, Biogeosciences, 5, 1425–1435, doi:10.5194/bg-5-1425-2008, 2008b.

Murray, B. J., Wilson, T. W., Dobbie, S., Cui, Z., Al-Jumur, S. M. R. K., Möhler, O., Schnaiter, M., Wagner, R., Benz, S., Niemand, M., Saathoff, H., Ebert, V., Wagner, S., and Karcher, B.: Heterogeneous nucleation of ice particles on glassy aerosols under cirrus conditions, Nat. Geosci., 3, 233–237, doi:10.1038/ngeo817, 2010.

Murray, B. J., Broadley, S. L., Wilson, T. W., Atkinson, J. D., and Wills, R. H.: Heterogeneous freezing of water droplets containing kaolinite particles, Atmos. Chem. Phys., 11, 4191–4207, doi:10.5194/acp-11-4191-2011, 2011.

Murray, B. J., O'Sullivan, D., Atkinson, J. D., and Webb, M. E.: Ice nucleation by particles immersed in supercooled cloud droplets, Chem. Soc. Rev., 41, 6519, doi:10.1039/c2cs35200a, 2012.

Nickovic, S., Vukovic, A., Vujadinovic, M., Djurdjevic, V., and Pejanovic, G.: Technical Note: High-resolution mineralogical database of dust-productive soils for atmospheric dust modeling, Atmos. Chem. Phys., 12, 845–855, doi:10.5194/acp-12-845-2012, 2012.

Nicolet, M., Stetzer, O., Lüönd, F., Möhler, O., and Lohmann, U.: Single ice crystal measurements during nucleation experiments with the depolarization detector IODE, Atmos. Chem. Phys., 10, 313–325, doi:10.5194/acp-10-313-2010, 2010.

Niedermeier, D., Shaw, R. A., Hartmann, S., Wex, H., Clauss, T., Voigtländer, J., and Stratmann, F.: Heterogeneous ice nucleation: exploring the transition from stochastic to singular freezing behavior, Atmos. Chem. Phys., 11, 8767–8775, doi:10.5194/acp-11-8767-2011, 2011.

Niemand, M., Möhler, O., Vogel, B., Vogel, H., Hoose, C., Connolly, P., Klein, H., Bingemer, H., DeMott, P., Skrotzki, J., and Leisner, T.: A particle-surface-area-based parameterization of immersion freezing on desert dust particles, J. Atmos. Sci., 69, 3077–3092, 2012.

O'Sullivan, D., Murray, B. J., Ross, J. F., and Webb, M. E.: The adsorption of fungal ice-nucleating proteins on mineral dusts: a terrestrial reservoir of atmospheric ice-nucleating particles, Atmos. Chem. Phys., 16, 7879–7887, doi:10.5194/acp-16-7879-2016, 2016.

Peckhaus, A., Kiselev, A., Hiron, T., Ebert, M., and Leisner, T.: A comparative study of K-rich and Na/Ca-rich feldspar ice-nucleating particles in a nanoliter droplet freezing assay, Atmos. Chem. Phys., 16, 11477–11496, doi:10.5194/acp-16-11477-2016, 2016.

Perlwitz, J. P., Pérez García-Pando, C., and Miller, R. L.: Predicting the mineral composition of dust aerosols – Part 1: Representing key processes, Atmos. Chem. Phys., 15, 11593–11627, doi:10.5194/acp-15-11593-2015, 2015.

Pinti, V., Marcolli, C., Zobrist, B., Hoyle, C. R., and Peter, T.: Ice nucleation efficiency of clay minerals in the immersion mode, Atmos. Chem. Phys., 12, 5859–5878, doi:10.5194/acp-12-5859-2012, 2012.

Prenni, A. J., Petters, M. D., Faulhaber, A., Carrico, C. M., Ziemann, P. J., Kreidenweis, S. M., and DeMott, P. J.: Heterogeneous ice nucleation measurements of secondary organic aerosol generated from ozonolysis of alkenes, Geophys. Res. Lett., 36, L06808, doi:10.1029/2008GL036957, l06808, 2009.

Pummer, B. G., Bauer, H., Bernardi, J., Bleicher, S., and Grothe, H.: Suspendable macromolecules are responsible for ice nucleation activity of birch and conifer pollen, Atmos. Chem. Phys., 12, 2541–2550, doi:10.5194/acp-12-2541-2012, 2012.

Rietveld, H. M.: A profile refinement method for nuclear and magnetic structures, J. Appl. Crystallogr., 2, 65–71, doi:10.1107/S0021889869006558, 1969.

Roberts, P. and Hallett, J.: A laboratory study of the ice nucleating properties of some mineral particulates, Q. J. Roy. Meteor. Soc., 95, 204–205, doi:10.1002/qj.49709540317, 1969.

Rogers, D. C.: Development of a continuous flow thermal gradient diffusion chamber for ice nucleation studies, Atmos. Res., 22, 149–181, 1988.

Schaefer, V. J.: The Production of Ice Crystals in a Cloud of Supercooled Water Droplets, Science, 104, 457–459, doi:10.1126/science.104.2707.457, 1946.

Schnell, R. C.: Ice Nuclei in Seawater, Fog Water and Marine Air off the Coast of Nova Scotia: Summer 1975, J. Atmos. Sci., 34, 1299–1305, doi:10.1175/1520-0469(1977)034<1299:INISFW>2.0.CO;2, 1977.

Schnell, R. C. and Vali, G.: Biogenic Ice Nuclei: Part I. Terrestrial and Marine Sources, J. Atmos. Sci., 33, 1554–1564, doi:10.1175/1520-0469(1976)033<1554:BINPIT>2.0.CO;2, 1976.

Schütz, L. and Sebert, M.: Mineral aerosols and source identification, J. Aerosol Sci., 18, 1–10, doi:10.1016/0021-8502(87)90002-4, 1987.

Steinke, I.: Ice nucleation properties of mineral dusts, PhD thesis, The Faculty of Physics and Astronomy, Institute of Environmental Physics, Heidelberg University, Heidelberg, 2013.

Stetzer, O., Baschek, B., Lüönd, F., and Lohmann, U.: The Zurich Ice Nucleation Chamber (ZINC)-A new instrument to investigate atmospheric ice formation, Aerosol Sci. Technol., 42, 64–74, doi:10.1080/02786820701787944, 2008.

Sullivan, R. C., Petters, M. D., DeMott, P. J., Kreidenweis, S. M., Wex, H., Niedermeier, D., Hartmann, S., Clauss, T., Stratmann, F., Reitz, P., Schneider, J., and Sierau, B.: Irreversible loss of ice nucleation active sites in mineral dust particles caused by sulphuric acid condensation, Atmos. Chem. Phys., 10, 11471–11487, doi:10.5194/acp-10-11471-2010, 2010.

Tobo, Y., Prenni, A. J., DeMott, P. J., Huffmann, A., McCluskey, C. S., Tian, G., Pöhlker, C., Pöschl, U., and Kreidenweis, S. M.: Biological aerosol particles as a key determinant of ice nuclei populations in a forest ecosystem, J. Geophys. Res. Atmos., 118, 1–11, doi:10.1002/jgrd.50801, 2013.

Vali, G.: Sizes of Atmospheric Ice Nuclei, Nature, 212, 384–385, doi:10.1038/212384a0, 1966.

Vali, G.: Quantitative Evaluation of Experimental Results an the Heterogeneous Freezing Nucleation of Supercooled Liquids, J. Atmos. Sci., 28, 402–409, doi:10.1175/1520-0469(1971)028<0402:QEOERA>2.0.CO;2, 1971.

Vali, G., DeMott, P. J., Möhler, O., and Whale, T. F.: Technical Note: A proposal for ice nucleation terminology, Atmos. Chem. Phys., 15, 10263–10270, doi:10.5194/acp-15-10263-2015, 2015.

Wang, B., Lambe, A. T., Massoli, P., Onasch, T. B., Davidovits, P., Worsnop, D. R., and Knopf, D. A.: The deposition ice nucleation and immersion freezing potential of amorphous secondary organic aerosol: Pathways for ice and mixed-phase cloud formation, J. Geophys. Res.-Atmos., 117, D16209, doi:10.1029/2012JD018063, 2012.

Welti, A., Lüönd, F., Stetzer, O., and Lohmann, U.: Influence of particle size on the ice nucleating ability of mineral dusts, Atmos. Chem. Phys., 9, 6705–6715, doi:10.5194/acp-9-6705-2009, 2009.

Welti, A., Lüönd, F., Kanji, Z. A., Stetzer, O., and Lohmann, U.: Time dependence of immersion freezing: an experimental study on size selected kaolinite particles, Atmos. Chem. Phys., 12, 9893–9907, doi:10.5194/acp-12-9893-2012, 2012.

Welti, A., Kanji, Z. A., Lüönd, F., Stetzer, O., and Lohmann, U.: Exploring the Mechanisms of Ice Nucleation on Kaolinite: From Deposition Nucleation to Condensation Freezing, J. Atmos. Sci., 71, 16–36, doi:10.1175/JAS-D-12-0252.1, 2014.

Wilson, T. W., Ladino, L. A., Alpert, P. A., Breckels, M. N., Brooks, I. M., Browse, J., Burrows, S. M., Carslaw, K. S., Huffman, J. A., Judd, C., Kilthau, W. P., Mason, R. H., McFiggans, G., Miller, L. A., Najera, J. J., Polishchuk, E., Rae, S., Schiller, C. L., Si, M., Temprado, J. V., Whale, T. F., Wong, J. P. S., Wurl, O., Yakobi-Hancock, J. D., Abbatt, J. P. D., Aller, J. Y., Bertram, A. K., Knopf, D. A., and Murray, B. J.: A marine biogenic source of atmospheric ice-nucleating particles, Nature, 525, 234–238, doi:10.1038/nature14986, 2015.

Zimmermann, F., Weinbruch, S., Schütz, L., Hofmann, H., Ebert, M., Kandler, K., and Worringen, A.: Ice nucleation properties of the most abundant mineral dust phases, J. Geophys. Res.-Atmos., 113, 1–11, doi:10.1029/2008JD010655, 2008.

Zolles, T., Burkart, J., Häusler, T., Pummer, B., Hitzenberger, R., and Grothe, H.: Identification of Ice Nucleation Active Sites on Feldspar Dust Particles, J. Phys. Chem. A, 119, 2692–2700, doi:10.1021/jp509839x, 2015.